SUB-GHZ PROPAGATION ALONG FREIGHT TRAINS FOR WIRELESS ONBOARD COMMUNICATIONS

A Thesis

by

DARIO HINOJOSA

Submitted in Partial Fulfillment of the

Requirements for the Degree of

MASTER OF SCIENCE IN ENGINEERING

Major Subject: Electrical Engineering

The University of Texas Rio Grande Valley
May 2026

SUB-GHZ PROPAGATION ALONG FREIGHT TRAINS FOR WIRELESS ONBOARD COMMUNICATIONS

A Thesis
by
DARIO HINOJOSA

COMMITTEE MEMBERS

Dr. Heinrich Foltz
Chair of Committee

Dr. Constantine Tarawneh
Co-Chair of Committee

Dr. Nantakan Wongkasem
Committee Member

May 2026

ABSTRACT

Hinojosa, Dario, Sub-GHz Propagation Along Freight Trains For Wireless Onboard Communications. Master of Science in Engineering (MSE), May 2026, 61 pp., 5 tables, 33 figures, 21 references.

With the increasing length of freight trains, maintaining reliable wireless communication for onboard sensors has become increasingly challenging. Sub-GHz communication bands are a promising solution due to their long-range capability and suitability for rural railway environments. This study analyzes radio wave propagation around freight railcars to evaluate path loss and determine how antenna polarization affects wireless communication performance.

Time-domain full-wave electromagnetic simulations were performed using simplified railcar models and later validated through field testing using a vector signal generator, vector network analyzer (VNA), and spectrum analyzer. Various antenna polarization configurations were evaluated within the Sub-GHz Long Range (LoRa) frequency band under worst-case railcar placement conditions.

Testing was conducted between opposite ends of a railcar to obtain the median and standard deviation of path loss across the operating band. Results demonstrate that antenna polarization and environmental reflections significantly influence received signal strength. These findings provide practical guidance for optimizing transmit power, antenna placement, and frequency hopping strategies for onboard wireless sensing systems in railroad applications.

DEDICATION

I dedicate this thesis to my friends and family, all of whom have helped me pursue my dream of becoming an electrical engineer. To my father, Eduardo Hinojosa-Salinas, for always showing me the importance of never giving up and for always providing for us. To my mother, Gloria Isabel Guerra, thank you for making sure we always had everything we needed and for always making us strive for success. To my brother Eduardo Hinojosa, thank you for always being a great role model and for always giving me important advice, even when I did not want to hear it. To my friends, thank you for always offering your support and always being willing to listen. Thank you all for turning me into the person I am today, as without you, none of this would have been possible.

ACKNOWLEDGEMENTS

I would like to give my deepest thanks to Dr. Heinrich D. Foltz. You have been an integral part of my engineering journey through your teaching and leadership, and I would not have been able to finish this thesis without your help. Dr. Foltz, you have been a great mentor, not just helping me grow as a student but also as a person.

Dr. Constantine Tarawneh, thank you for the opportunity to work with you at both MECIS and the UTCRS. These experiences have helped shape my life in more ways than I can count. You have shown me how to be a leader, a hard worker, and a great person.

Dr. Nantakan Wongkasem, thank you for always being there for your students and me. Thank you for sharing your passion for engineering; without it, I would never have unlocked my full potential by connecting the subjects to create new ideas.

I would like to thank everyone from both centers, especially Rogelio, Amanda, and Anahi. You guys have made my time here wonderful and have helped me grow as a person in ways I did not think possible. I know you will all do great things.

I would like to thank Patrick Johnson and Ironhorse for allowing me to use their railcars and Hum Industrial Technologies, Inc., for providing sample wireless devices.

Lastly, I would like to thank both the UTCRS, through the USDOT UTC Program under Grant No. 69A3552348340, and the NSF CREST Center for Multidisciplinary Research Excellence in Cyber-Physical Infrastructure Systems (CREST-MECIS) for their financial support through the NSF Award No. 2112650

DISCLAIMER

The contents of this thesis reflect the views of the authors who are responsible for the facts and the accuracy of the information presented herein. This document is disseminated under the sponsorship of the National Science Foundation (NSF) and the United States Department of Transportation (USDOT), in the interest of information exchange. NSF and USDOT assume no liability for the contents or use thereof.

TABLE OF CONTENTS

LIST OF TABLES

LIST OF FIGURES

Page

CHAPTER I

INTRODUCTION

Currently, the rail industry relies on reactive monitoring systems such as wayside detectors to prevent derailments caused by railcar wheels and bearings. While these systems work to identify impending failures, due to the sparsity of installations, they may miss sudden events such as bearing seizures that can cause burnoff in less than one minute. They also have limited sensitivity for detecting defects in their early stages of development since they rely on remote sensing. Motivated by this, the University Transportation Center for Railway Safety (UTCRS) has developed an onboard wireless sensor for proactive bearing condition monitoring [1]. This sensor collects vibration data close to the bearing and relays it to a wireless hub or gateway. The gateway is an electronic device that gathers information from other devices, in this case, the onboard sensors, which connect to it wirelessly. This device then sends the acquired information to the end user. This gateway uses the LoRa communication protocol to send and receive data from the sensors. The motivation for this study is to examine LoRa and test its limitations in rail applications. This is done to more accurately determine the transmit power required for a given sensor position and data rate, and thus reduce the power consumption of wireless communication systems, therefore increasing battery life, improving reliability, and ensuring that the device is always able to communicate with its receiver. To accomplish this, simulations in CST Studio Suite were performed to determine communication performance, and testing on rolling stock was conducted to validate the simulation results.

The freight rail industry plays a vital role in supporting the North American economy by transporting large volumes of raw materials and finished products, effectively connecting industrial, agricultural, and commercial regions. The freight rail network is broadly acknowledged to be the "largest, safest, and most cost-efficient" transportation system by the Federal Railroad Association (FRA) [1]. Derailments pose a safety risk not only to the freight rail industry but also to surrounding communities. Critical railcar components, such as tapered roller bearings, are known to be among the primary contributors to mechanical failure, often resulting in derailments [2]. Prioritizing safety within the rail industry begins with proper inspection and maintenance of railcar components. Proper reconditioning of tapered roller bearings is essential for minimizing risk of derailments. Incorporating a post-reconditioning Nondestructive Evaluation (NDE) method, via Eddy Current Array (ECA), can further enhance reliability by identifying near-surface or subsurface defects that may be missed during standard reconditioning procedures.

1.1 Bearing Derailments

Currently, bearing failure derailments account for 1.1% of U.S. train derailments in 2025, according to the Federal Railroad Administration (FRA) [2]. While derailments caused by failed bearings are not very common, when they occur, they tend to be catastrophic. Since most failures are caused by overheating, the bearing melts onto the train axle and ceases rotation of the wheel, which may lead to several adjacent railcars to derail depending on the train traveling speed, with some of these cars might be carrying hazardous material. A recent catastrophic derailment caused by a bearing failure was the East Palestine, Ohio, derailment on Feb 3, 2023. According to the National Transportation Safety Board (NTSB), "[Norfolk Southern] estimated the damage to equipment to be about $3.4 million" [3]. While equipment costs were high, they paled in comparison to the total damages, which amounted to about $2.2 billion.

1.2 Bearing Defect Detection

Bearing defect detection has multiple methods, each with its strengths and weaknesses. In the United States of America, wayside bearing condition-monitoring systems dominate the market. Stepping further into these methods, there are two common systems, Hot Bearing (or Box) Detectors (HBDs) and Acoustic Bearing Detectors (ABDs). These systems use sensors to detect when a bearing reaches predetermined thresholds for each system and promptly notify the train conductor to stop the train and replace the wheel and axle assembly before resuming operation. These systems are installed parallel to the tracks to monitor bearing conditions as the railcar passes the device.

1.2.1 Types of Defects

Currently, HBDs are the most common wayside detectors with over 6,000 units in North America and are typically placed 40 to 64 km (25 to 40 mi) apart [4]. HBDs utilize infrared sensors to measure the bearing operating temperature. When bearings operate at temperatures that are 94.4°C (170°F) above ambient conditions or 58.3°C (105°F) hotter than the mate bearing that shares the same axle, the HBD will trigger an alarm that notifies the train operators, and this will lead to the immediate stopping of the train so the suspect axle can be removed from service [5]. Some railroads use a more conservative method to detect potential failures. In this case, the railroads will scan for "warm trending" bearings. These bearings operate at significantly higher temperatures than the average temperature of all the bearings on the same side of the train [5]. This results in warm-trended bearings flagged for inspection without triggering HBD alarms. A picture of an HBD system can be seen below in Figure 1.

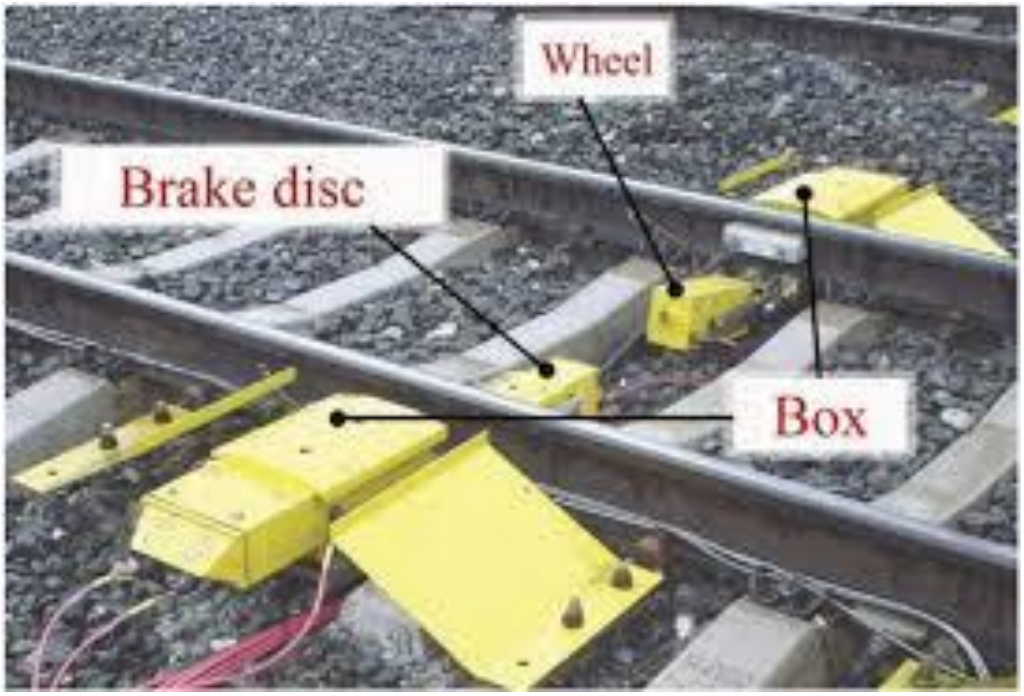

Figure 1: Hot Bearing (or Box) Detector (HBD) [6]

1.2.2 Trackside Acoustic Detection Systems

Acoustic Bearing Detectors (ABDs) are another type of wayside detection systems currently utilized by railroads. ABDs in North America consist of two different types: Trackside Acoustic Detection Systems (TADS™) and RailBAM®. Each of these technologies utilize acoustics to determine the deterioration of tapered roller bearings. TADS™ are installed on the side of the track and use microphones to capture the acoustic emissions of passing trains. The sensor would notify the train operator if the identified defects are severe enough for inspection. TADS™ were originally able to detect small defects; however, it quickly became apparent that the replacements were too costly in comparison to the remaining serviceable lifespan. As a result, the TADS™ algorithm was modified to detect only high-risk bearings. An example is a "growler," which is a bearing that emits a low-frequency sound when approximately 90% of the bearing raceways have spalled. Following the updated algorithm, a study was conducted, and it was found that some high-risk bearings were not detected by TADS™ [7]. As of March 2017, only 19

TADS™ were in operation nationwide, making it unlikely that most bearings would go through this system [8]. A picture of a TADS™ installation is pictured in Figure 2.

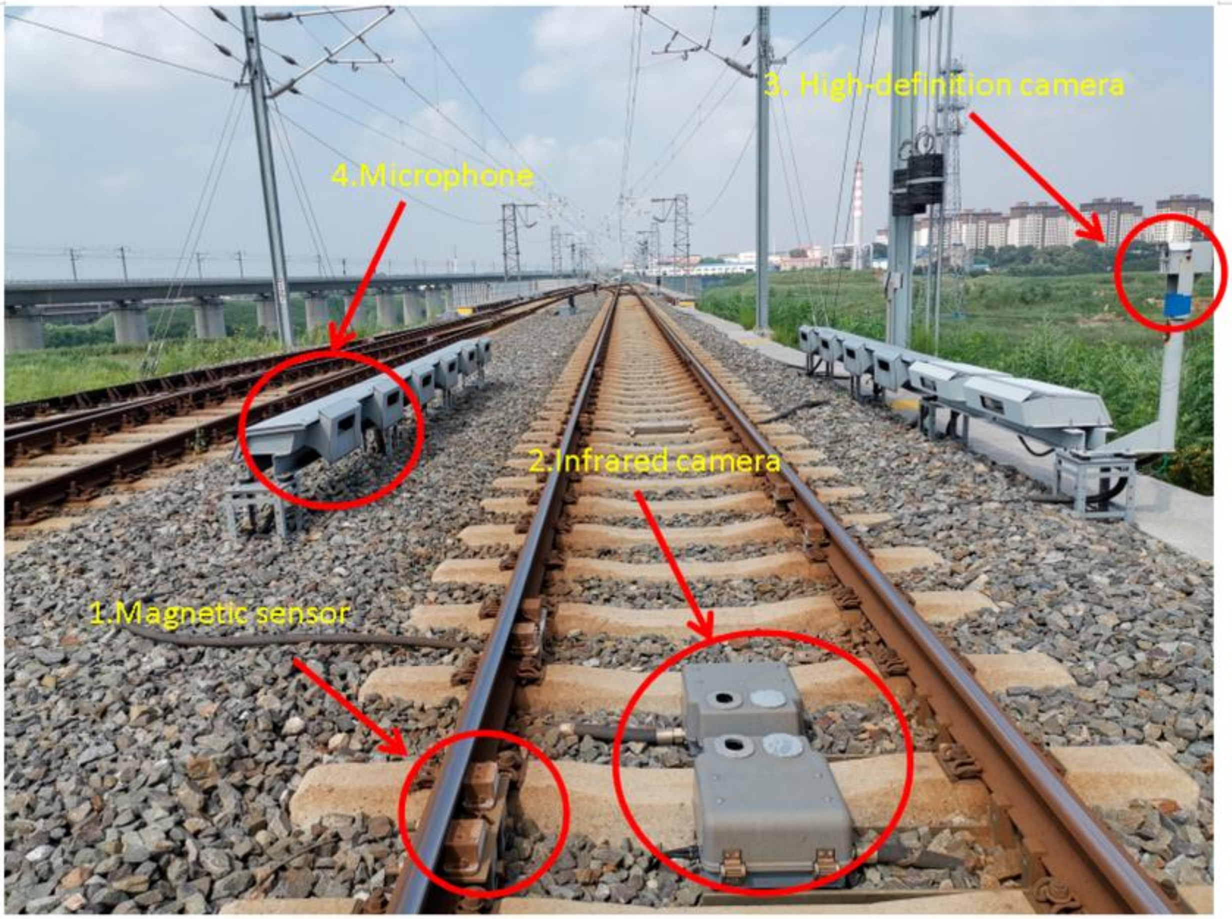

Figure 2: Trackside Acoustic Detection System (TADS™) [9]

Like TADS™, RailBAM® uses a microphone array on the side of the tracks to determine bearing defects. The main difference between RailBAM® and TADS™ is that RailBAM® can provide predictive trend information on bearing severity [10]. RailBAM® records the acoustic history of a bearing every time a train passes by the system, allowing the railcar owners to develop a maintenance plan to reduce costly inspections. The main limitation of this system is the number of deployed units: as of March 2017, only 20 RailBAM® devices had been installed in East and Midwest locations in the United States, with only a small percentage of railcars passing through this system, like the case in TADS™ [4], [8]. A picture of a RailBAM® installation is shown in Figure 3.

Figure 3: RailBAM® [11]

1.3 Wireless Onboard Sensing

The University Transportation Center for Railway Safety (UTCRS) developed a wireless onboard bearing condition monitoring system capable of continuously monitoring bearing health directly on the railcar [12]. The system mounts sensors directly onto the bearing adapter, allowing vibration and temperature data to be collected close to the rolling elements. Figure 4 shows the UTCRS wireless onboard sensor module mounted to a freight railcar bearing adapter.

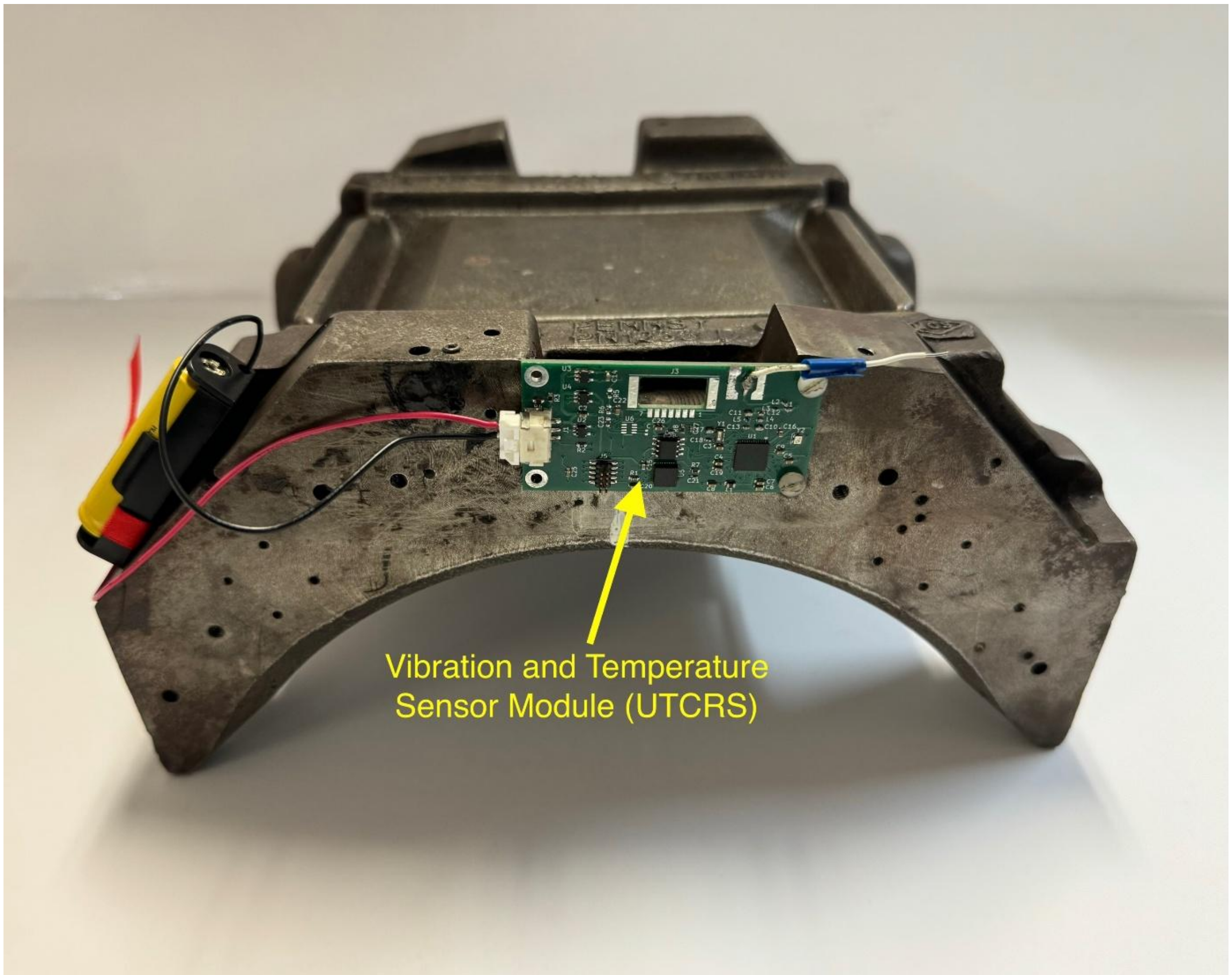

Figure 4: UTCRS Wireless Onboard Sensor

Shortly after the development of the UTCRS wireless sensors, UTCRS licensed the technology to Hum Industrial Technologies, Inc., where it was developed into the Hum Boomerang™. This device is battery-operated and uses the Long Range (LoRa) communication protocol to transmit bearing health data. It does this through a multitude of sensors. These sensors are coupled to an algorithm to prevent derailments caused by bearing failures before they occur. Figure 5 shows one of the earlier versions of the Hum Boomerang™ (Version 5.0) mounted to a railcar bearing adapter.

Figure 5: Hum Boomerang™ Version 5.0 (V5) [13]

The wireless sensor module contains accelerometers, temperature-sensing components, and a wireless communication interface that transmit collected data to a central gateway for processing and analysis. According to Tarawneh et al., vibration-based monitoring provides an advantage because vibration signatures can detect localized defects such as pits, cracks, and spalls during the early stages of failure progression [12]. The UTCRS system was validated through both laboratory and field testing at the Transportation Technology Center, Inc. (TTCI) in Pueblo, Colorado, in spring of 2015. Results showed that the wireless onboard monitoring system could accurately identify defects on both cone and cup raceways under varying operating speeds and loading conditions while the train remained in service [12].

Power consumption is one of the most important considerations in wireless onboard sensing systems because the sensor modules are battery-powered and are expected to operate for extended periods (over 6 years) with minimal maintenance. Excessive transmit power reduces battery life and increases maintenance requirements due to more frequent unit replacement or servicing. For this reason, determining the minimum transmit power required to maintain reliable communication is critical. Operating at the minimum effective transmit power reduces overall energy consumption, extends operational lifetime, minimizes interference with nearby wireless systems, and improves the long-term reliability and practicality of wireless onboard monitoring systems for freight rail applications.

1.4 Thesis Overview

As stated earlier, all simulations will be conducted in CST Studio Suite, a software used to model electromagnetic components and their interactions. CST Studio Suite was chosen for its ease of use, compared with other electromagnetic software such as Ansys HFSS, and for its availability. Various simulations were conducted, including modeling individual antennas. Individual modeling was used to optimize a half-wave dipole antenna to mimic sensor antennas. One reason for this choice is that dipole antennas are common, isotropic/omnidirectional, and well understood. However, the more important reason is that the antennas in use on the current generation of wireless onboard sensors are reduced-sized but impedance matched miniature dipoles with similar characteristics. Antenna-to-antenna performance from 1-on-1 helped identify the best location for the gateway.

Lastly, field testing was conducted to verify simulation results. The field test was also used to identify factors not accounted for in the simulations. Field tests were conducted with the support of the Rio Valley Switching Company, a local short-line railroad owned and operated by Ironhorse Resources. These tests were conducted by placing a signal generator in an area to mimic the gateway position and a spectrum analyzer, a device used to test signal strength across a frequency range.

CHAPTER II

LITERATURE REVIEW

2.1 Introduction

The increasing demand for real-time monitoring of freight train components has led to the development of onboard wireless sensor networks capable of continuously assessing equipment health. Reliable wireless communication is essential for the successful deployment of these systems, particularly in the challenging electromagnetic environment created by long freight trains composed of metallic railcars. This chapter reviews the relevant literature on Low Power Wide Area Network (LPWAN) technologies, with a focus on LoRa and Sub-GHz communication, radio wave propagation in complex environments, antenna design considerations, and the safety concerns raised by the East Palestine, Ohio, derailment on February 3, 2023. The synthesis of these studies establishes the foundation for the simulation and experimental investigations presented in this thesis.

2.2 Low Power Wide Area Network Technologies

Low Power Wide Area Network (LPWAN) technologies have emerged as a key enabler of large-scale Internet of Things (IoT) deployments. These technologies are designed to provide long-range communication while maintaining low power consumption and minimal infrastructure requirements. Among the various LPWAN solutions, LoRa has gained significant attention due to its robustness and flexibility in unlicensed Sub-GHz frequency bands.

Centenaro et al. [14] provide a comprehensive overview of LoRa technology, describing its use of chirp spread spectrum modulation to achieve high receiver sensitivity and resilience to interference. The authors demonstrate that LoRa systems can support communication over several kilometers while maintaining low energy consumption, making them suitable for applications in remote and infrastructure-limited environments. Complementing this work, Raza et al. [15] present a broader survey of LPWAN technologies, highlighting the trade-offs between coverage, data rate, and energy efficiency. Their analysis indicates that LoRa offers a favorable balance of these characteristics, positioning it as an attractive solution for railway sensor networks where long communication distances and low maintenance requirements are essential.

2.3 Sub-GHz Radio Propagation in Metallic Environments

The propagation of radio waves in railway environments is influenced by the extensive use of metallic materials in railcar construction. Sub-GHz frequency bands are particularly advantageous for such environments due to their lower free-space path loss and enhanced diffraction capabilities compared to higher-frequency systems. These properties enable improved signal penetration and more reliable communication over extended distances.

Rappaport [16] provides a foundational treatment of wireless propagation mechanisms, including reflection, diffraction, and scattering, all of which are highly relevant to freight trains. The presence of large conductive surfaces can lead to significant multipath propagation, resulting in constructive and destructive interference patterns. Additionally, the elongated geometry of freight trains can create waveguiding effects, allowing electromagnetic waves to propagate along the length of the train. Understanding these propagation characteristics is essential for optimizing antenna placement and ensuring reliable communication between onboard sensors and gateways.

Empirical and simulation studies reported in the literature emphasize the importance of antenna positioning and polarization in mitigating signal degradation in complex environments. These findings support the need for detailed electromagnetic modeling and experimental validation, as undertaken in this thesis.

2.4 Antenna Design Considerations for Onboard Sensor Networks

Antenna design plays a critical role in determining the performance of wireless communication systems. Dipole antennas are commonly employed in sensor network applications due to their simplicity, omnidirectional radiation pattern, and well-understood electromagnetic behavior. Balanis [17] provides an authoritative reference on antenna theory, detailing the principles governing resonant frequency, impedance matching, radiation patterns, and bandwidth. These principles form the basis for the antenna design and optimization processes used in this research.

The interaction between antennas and their surrounding environment is another important consideration. The proximity of conductive structures, such as steel railcars, can detune antennas and alter their radiation characteristics, potentially reducing communication efficiency. Rappaport [16] discusses the impact of environmental factors on wireless system performance, emphasizing the necessity of incorporating these effects into both simulation and measurement campaigns. Consequently, electromagnetic simulation tools, such as CST Studio Suite, are essential for accurately predicting antenna behavior in realistic railway scenarios.

2.5 Safety Motivation: The East Palestine Derailment

The importance of reliable onboard monitoring and communication systems is underscored by the Norfolk Southern freight train derailment that occurred in East Palestine, Ohio, on February 3, 2023. According to the National Transportation Safety Board (NTSB), the derailment was initiated by the failure of an overheated wheel bearing, which ultimately led to the derailment of multiple railcars [3]. Several of the derailed cars were transporting hazardous materials, including vinyl chloride, resulting in hazardous materials release and a subsequent controlled vent and burn operation.

The incident prompted the evacuation of nearby communities and caused significant environmental and economic impacts. The NTSB investigation highlighted that, although wayside detectors properly captured the increase in bearing operating temperature prior to the derailment, the rapid progression of the failure demonstrated the need for enhanced proactive monitoring capabilities and improved communication systems [3]. Continuous onboard sensing, combined with reliable wireless data transmission, has the potential to enable earlier detection of hazardous conditions, thereby reducing the likelihood of similar catastrophic events in the future.

2.6 Radio Propagation in Railway Environments

Wireless propagation in railway environments poses several challenges due to large metallic structures, varying terrain, and environmental obstructions. Understanding these effects is essential when designing reliable onboard communication systems for freight trains operating in diverse environments.

Sanches et al. [18] investigated radio propagation within railway corridors surrounded by dense forests at 460 MHz. Their work combined field measurements with propagation modeling to evaluate signal attenuation caused by vegetation and terrain along railway tracks. The study demonstrated that foliage density and terrain irregularities can significantly reduce received signal strength, particularly over long communication distances. Despite these losses, lower-frequency signals in the Sub-GHz range maintained stronger propagation performance compared to higher-frequency systems due to reduced path loss and improved diffraction characteristics.

These findings are particularly relevant to freight rail applications operating in rural or forested environments, where communication links may span long distances with limited infrastructure.

2.7 RF Propagation for Wireless Sensor Networks

Wireless sensor networks require reliable communication links despite operating in environments that may contain obstructions, interference sources, and significant multipath propagation. Propagation studies for wireless sensor networks therefore provide important insights into antenna behavior, signal attenuation, and network reliability.

Sharif and Hempel [19] investigated RF propagation characteristics for wireless sensor networks with emphasis on signal attenuation and environmental effects in practical deployment scenarios. Their study demonstrated that propagation behavior is highly dependent on antenna orientation, surrounding materials, and deployment geometry. The authors showed that multipath fading and polarization mismatch can substantially degrade communication performance, particularly in environments containing reflective surfaces and physical obstructions.

The conclusions presented by Sharif and Hempel closely relate to the propagation mechanisms investigated in this thesis. Freight railcars create a highly reflective electromagnetic environment where antenna polarization and placement strongly influence communication reliability. Similar to the findings reported in their work, the simulations and field measurements presented here demonstrate that cross-polarized antenna configurations significantly outperform co-polarized arrangements.

2.8 Outdoor-to-Indoor and Indoor-to-Indoor Propagation in High-Speed Trains

Wireless communication systems deployed in railway applications must also account for propagation between different regions of the train structure. This includes communication between external infrastructure and internal passenger compartments, as well as communication between multiple enclosed areas within the train itself.

Research on propagation modeling for outdoor-to-indoor and indoor-to-indoor wireless links in high-speed trains investigated signal behavior through train car structures and passenger environments [20]. The study analyzed attenuation caused by train walls, windows, and internal partitions, and evaluated the impact of multipath propagation within enclosed railcars. The results showed that train car materials significantly influence signal penetration and propagation behavior, particularly at higher frequencies where attenuation through conductive structures becomes more severe.

The findings from this work further support the importance of using lower-frequency communication systems in railway environments. Sub-GHz frequencies provide improved penetration and reduced attenuation compared to higher-frequency systems, making them more suitable for communication around metallic railcars.

2.9 Research Gap and Contribution

Despite the extensive body of research on LPWAN technologies and wireless propagation, there remains a limited understanding of Sub-GHz signal behavior specifically along the length of freight trains. Much of the existing literature focuses on general wireless environments or high-speed passenger rail systems, with comparatively little attention given to the unique structural and operational characteristics of long freight trains. Furthermore, there is a scarcity of studies that integrate electromagnetic simulations with field measurements to validate propagation models in these environments.

Several studies have investigated radio propagation in railway-related environments. Sanches et al. [18] examined radio propagation in railway corridors through dense forests at 460

MHz using both field measurements and propagation modeling. Their work demonstrated that lower-frequency Sub-GHz signals maintain favorable propagation characteristics in obstructed railway environments due to reduced path loss and improved diffraction. However, the study primarily focused on large-scale propagation along railway corridors and environmental attenuation caused by terrain and vegetation. In contrast, the present research investigates short-range onboard communication along freight trains, where the dominant propagation mechanisms are reflections, diffraction, and multipath interactions produced by metallic railcars.

Sharif and Hempel [19] investigated RF propagation characteristics for wireless sensor networks in rail-related environments, with particular emphasis on antenna orientation, deployment geometry, and multipath fading effects at 2.4 GHz. Their results demonstrated that antenna polarization and surrounding structures significantly influence received signal strength and communication reliability. These findings are highly relevant to freight rail applications, where large conductive railcar surfaces create complex propagation environments. However, their work focused on wireless propagation at 2.4 GHz, where signal attenuation and obstruction losses are generally greater than those encountered at Sub-GHz frequencies. In contrast, the present thesis investigates Sub-GHz LoRa propagation along freight trains, where lower operating frequencies provide reduced path loss, improved diffraction, and enhanced propagation around metallic structures. Additionally, this research combines CST Studio Suite electromagnetic simulations with experimental field measurements to evaluate propagation performance in realistic freight rail environments.

Additional research on propagation modeling for outdoor-to-indoor and indoor-to-indoor wireless links in high-speed trains investigated signal attenuation through train structures and enclosed passenger environments [20]. The study demonstrated that train car materials and internal geometry significantly influence signal penetration and multipath behavior. While these findings contribute to the understanding of wireless propagation in railway systems, the focus was primarily on passenger rail communication involving train interiors. In contrast, this thesis examines external onboard communication between sensor nodes mounted on freight railcar bogies and gateway antennas positioned elsewhere on the train. Consequently, the propagation mechanisms considered in this work are dominated by external reflections and diffraction around metallic freight structures rather than indoor propagation within passenger compartments.

This thesis addresses these gaps by investigating the propagation of Sub-GHz LoRa signals along freight trains through a combination of CST Studio Suite simulations and experimental field testing. The research aims to determine optimal antenna configurations and gateway placements, thereby contributing to the development of reliable onboard wireless sensor networks capable of enhancing rail safety and operational efficiency.

2.10 Summary

This chapter has reviewed the literature relevant to the development of onboard wireless communication systems for freight trains. The discussion highlighted the advantages of LPWAN technologies, particularly LoRa, and the favorable propagation characteristics of Sub-GHz frequency bands in metallic environments. Foundational works on wireless propagation and antenna theory provided the theoretical basis for the simulation and experimental methodologies employed in this study. The East Palestine derailment was presented as a significant safety motivation, emphasizing the need for continuous onboard monitoring supported by robust wireless communication. The identified research gaps establish the foundation for the contributions of this thesis.

CHAPTER III

METHODOLOGY

3.1 Antenna Design

3.1.1 Frequency determination for dipole antenna size

To determine the optimal placement for Sub-GHz wireless communications systems, simulations were a good starting point, given that they can be more efficiently performed without the complexity of scheduling field testing with an actual railcar. Moreover, simulations enable control and isolation of different physical effects that cannot easily be separated in the field. The simulations are later used for comparison with the acquired experimental results from the conducted field testing.

All simulations are modeled using dipole antennas with a center frequency of 915 MHz. This frequency was selected as the center frequency for all dipole antennas, since the testing frequency range is from 900 MHz to 930 MHz, and includes the 902-928 MHz ISM (Industrial Scientific and Medical) frequency band used by LoRa devices configured for use in the United States. All dipole antennas were initially dimensioned by making the length of the dipole antenna $\lambda/2$, where λ is the wavelength of the center frequency. Since this is an approximate formula that does not account for proximity to conducting objects, the length was then optimized in the simulations to bring the resonance frequency within the desired band.

Applying the calculated wavelength to $\lambda/2$ yields 16.39 cm. To accommodate the antenna feed, 1 cm is subtracted from the center of the antenna, resulting in 15.39 cm for the total dipole length. Dividing this value by 2 yields the length of each monopole, which is about 7.70 cm.

3.1.2 S-Parameters

S-parameters indicate both the reflection coefficient and the transmission coefficient. S-parameters are denoted by the variables $S_{11}, S_{12}, S_{21}, S_{22}$, where S_{11} represents the reflection coefficient, indicating the amplitude of the signal reflected to the transmitting device relative to the incident amplitude, and S_{21} represents the transmission coefficient, indicating the amplitude of the received signal, again relative to the incident amplitude. They are normally represented in a matrix as seen below:

$$\begin{bmatrix} S_{11} & S_{12} \\ S_{21} & S_{22} \end{bmatrix}$$

The power reflected and transmitted, relative to incident power, are given by $|S_{11}|^2$ and $|S_{21}|^2$, respectively [17]. For S_{11}, lower (more negative) decibel (dB) values are preferable, as they correspond to reduced power reflection. Since decibels are logarithmic, an antenna with a -10 dB at a given frequency indicates that only 10% of the power is lost or reflected. In contrast, for S_{21}, which indicates the transmission coefficient, higher (less negative) dB values are preferable, as they correspond to higher power absorption. An example of S-parameters for a short antenna-to-antenna link is shown in Figure 6.

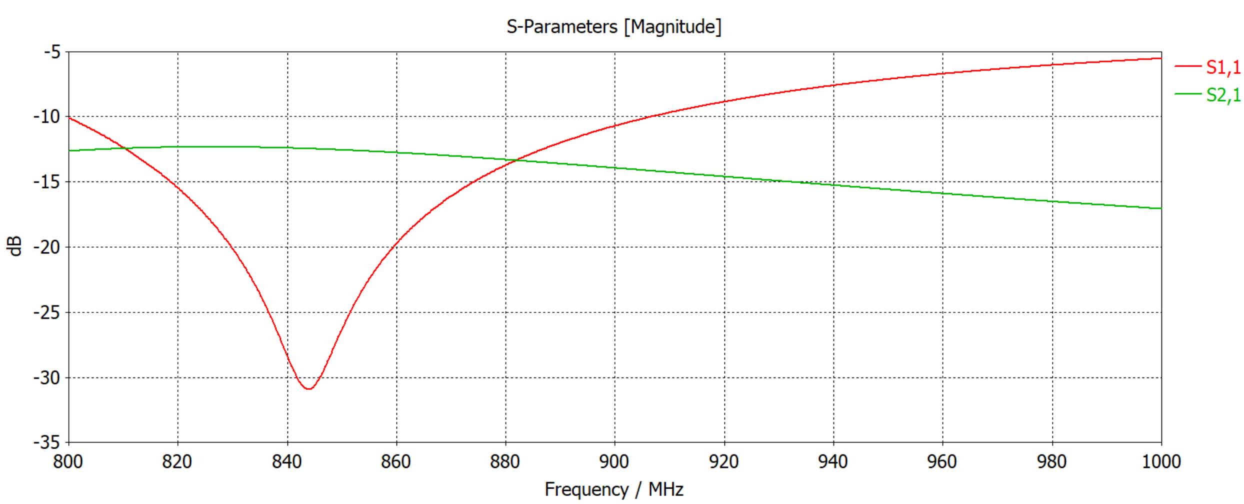

Figure 6: S-Parameter Example

3.1.3 MATLAB Antenna Design

To verify these results, MATLAB was employed to optimize a 915 MHz antenna for use in propagation modeling and field testing. The Antenna Designer tool was used to select a cylindrical dipole, set the frequency to 915 MHz, and specify copper as the dipole conductor. When validating the results, MATLAB reported 15.39 cm as the dipole length, as shown in Figure 7. After verifying the antenna dimensions, the resonant frequency had to be measured. S-parameters were utilized to evaluate the antenna. The S-parameters showed that the 15.39 cm antenna has a center frequency of 880 MHz, which is shown below in Figure 8. To compensate for this, the antenna had to be shrunk. To determine how much to shrink the antenna, the original antenna length is multiplied by the ratio of the original center frequency and the desired center frequency, as seen in Eq. (1):

$$L_c = L \times \frac{f}{f_c} \tag{1}$$

where L_c is the calculated length for a center frequency, f_c is the desired center frequency, L is the original antenna length, and f is the original frequency. Applying the values results in a new length of 14.8 cm. Changing the antenna length to 14.8 cm resulted in the desired center frequency of 915 MHz, as can be seen in Figure 9.

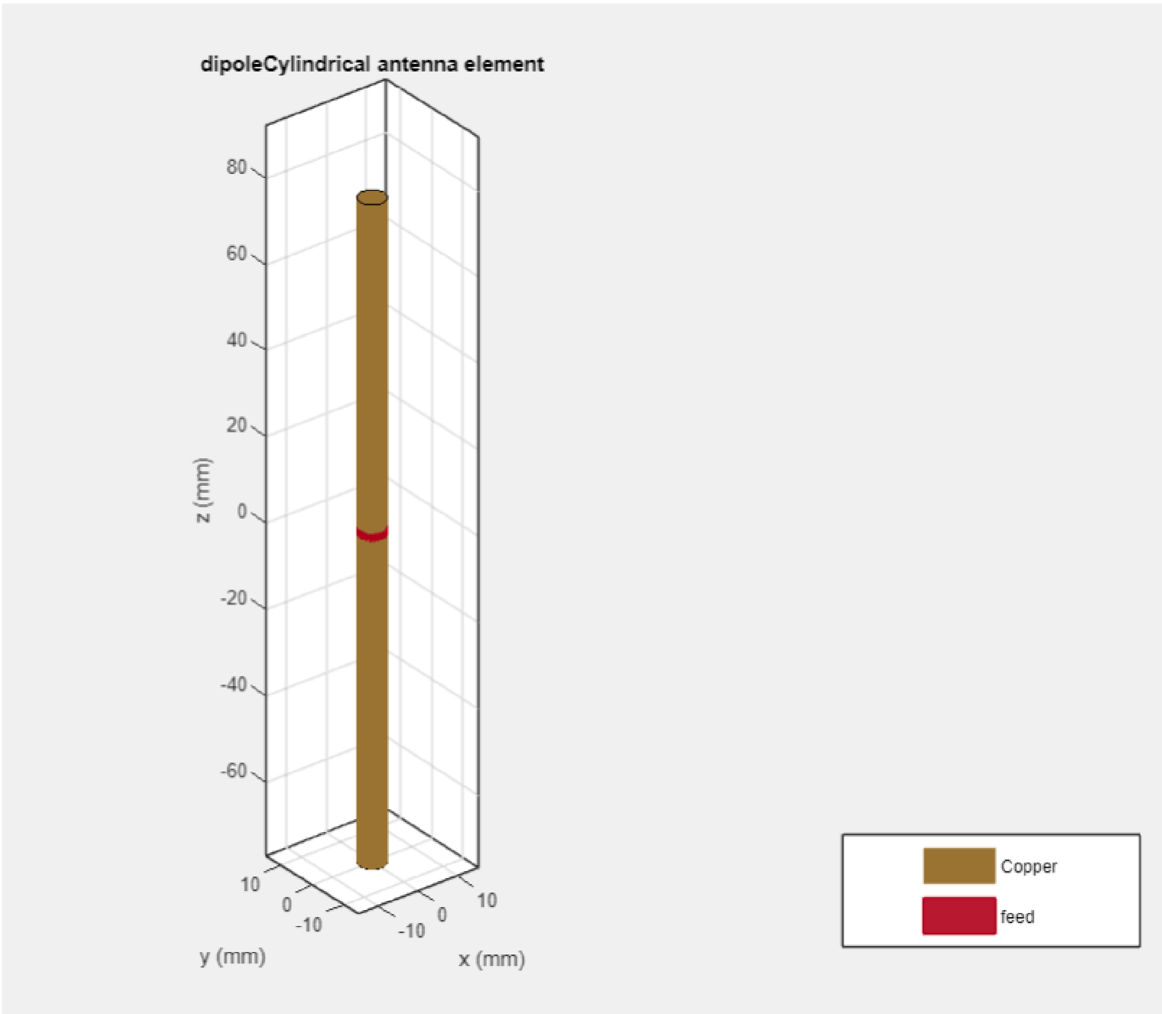

Figure 7: Original MATLAB Dipole Antenna

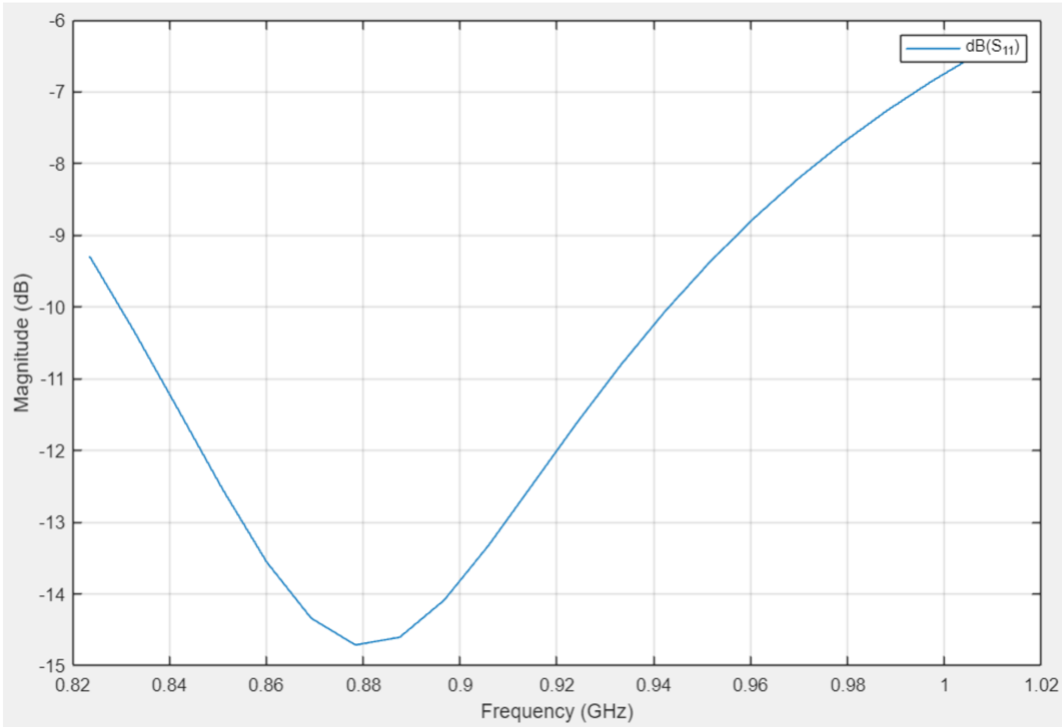

Figure 8: Original MATLAB Dipole Antenna S-parameters (15.39 cm)

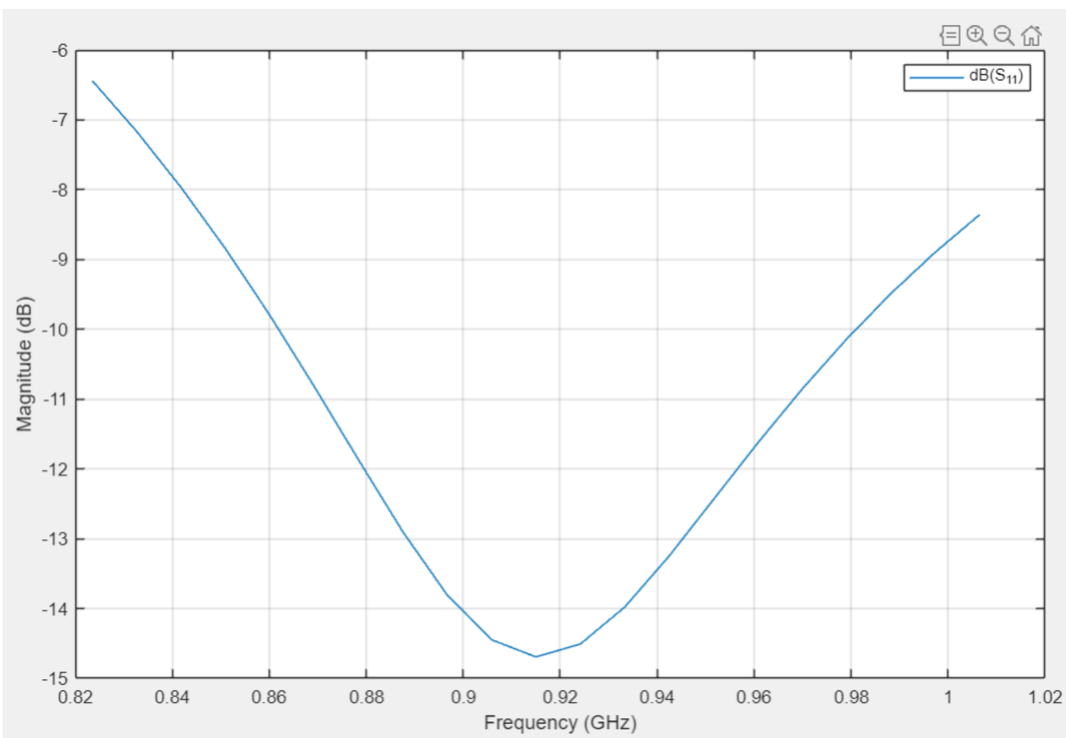

Figure 9: MATLAB Antenna Updated Dimensions (14.8 cm)

3.1.4 CST Studio Suite Design

After modeling the antenna in MATLAB, it was then simulated on CST Studio Suite to verify its performance. In CST Studio Suite, the antenna was modeled using optimized dimensions from MATLAB. This was done using the CST Studio Suite parameter function, which allows quick tuning of parameters and the creation of a discrete port with an impedance of 50 Ω, the standard for most antennas. The discrete port was placed at the location of the 1 cm gap, mimicking the feed that the discrete port simulates. Following this, the antenna performance was tested using time-domain analysis with a hexahedral mesh and an accuracy of -40 dB. Time domain analysis was selected due to the size of the structures being tested. Time-domain analysis examines how a signal evolves over time. This process resulted in a center frequency of 885 MHz, as presented in Figure 10. This result happened because the antenna diameter was changed to 1 cm, which was done to achieve higher bandwidth and to simplify the CST Studio Suite model. Therefore, to adjust the center frequency of the antenna to 915 MHz, its length was recalculated using Eq. (1), which resulted in an antenna length of 14.2 cm. From there, the CST Studio Suite parameters were updated, and the S-parameters were recalculated. The new center frequency was at 914 MHz, as shown in Figure 11. To finalize the design Eq. (1) was utilized again, resulting in a new length of 14.18 cm. The S-parameters indicate that the center frequency was 915 MHz, as shown in Figure 12. A finalized version of the antenna, including its dimensions, can be seen in Figure 13. This antenna would then be utilized for the rest of this study.

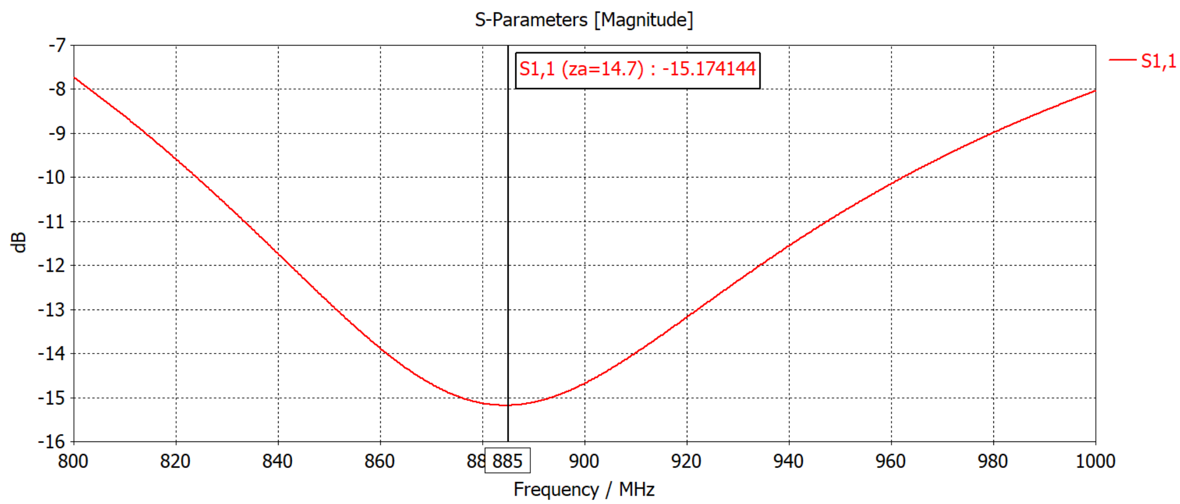

Figure 10: S-parameters for Dipole Antenna with a Length of 14.7 cm

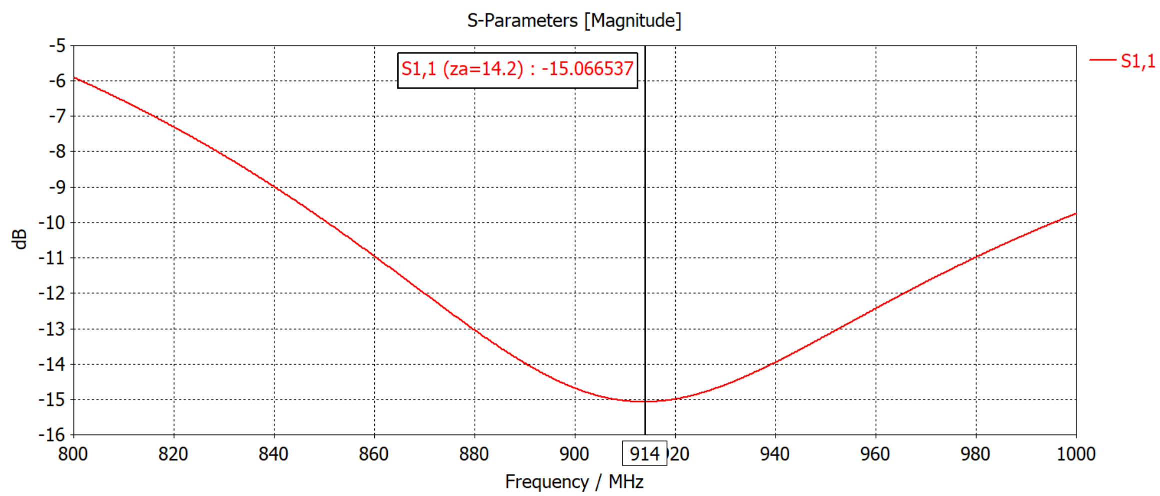

Figure 11: S-parameters for Dipole Antenna with a length of 14.2 cm

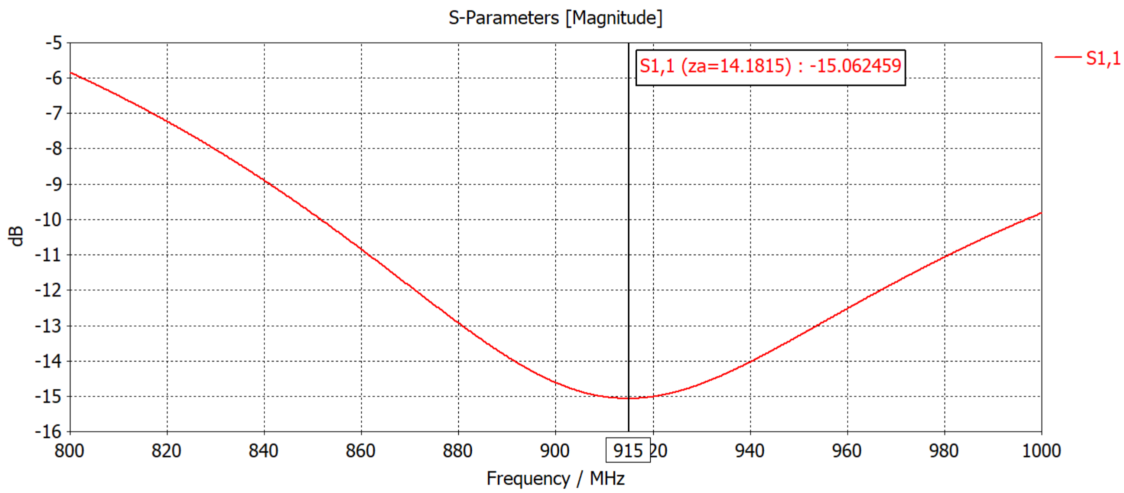

Figure 12: S-parameters for Dipole Antenna with a length of 14.18 cm

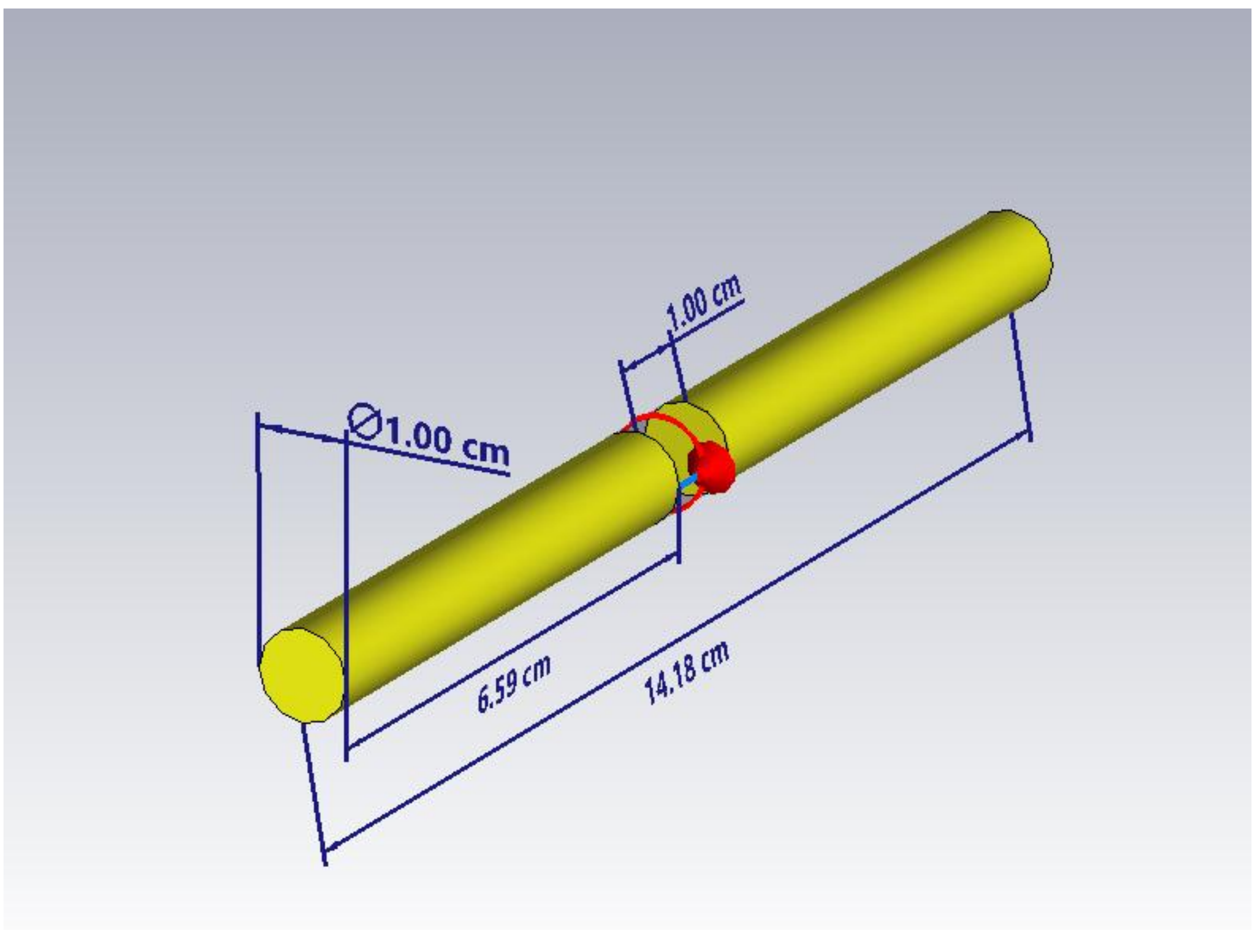

Figure 13: Finalized Dipole Antenna with Dimensions

CHAPTER IV

SIMULATION

4.1 Modeling the Train Car

After finalizing the dipole antenna design, a railcar model was developed to evaluate antenna performance in a realistic freight environment. A photograph of a typical boxcar is provided in Figure 14. Dimensions for the railcar were obtained through direct measurements of a boxcar provided by a local short-line railroad. A boxcar was selected because of its fully enclosed metallic structure, which presents a challenging electromagnetic environment for wireless communication.

Figure 14: Boxcar with Dimensions and Sensor Placement Locations [21]

The measured dimensions were 12.2 m (40 ft) in length, 3.0 m (9.84 ft) in width, and 2.34 m (7.67 ft) in height. A wall thickness of 0.64 cm (0.25 in) was used to approximately represent the railcar structure.

To accommodate the large dimensions of the railcar, the default CST Studio Suite units were modified. The length unit was changed from millimeters to centimeters, and the frequency unit was changed from gigahertz to megahertz. All other units remained unchanged.

The railcar material was modeled using Steel–1008 from the CST Studio Suite material library. This material has a relative permeability of approximately 1 at high frequencies, such as 900 MHz, and an electrical conductivity σ of 7.69 MS/m. Although Steel–1008 does not precisely match the steel composition used in freight railcars, its electromagnetic properties closely approximate those of typical structural steel. Any differences in magnetic permeability are expected to produce only minor shifts in resonant frequency, with negligible influence on overall antenna gain and propagation behavior. At 900 MHz, the skin depth of conductive metals is on the order of only a few microns, meaning that negligible electromagnetic energy penetrates through the steel railcar walls. As a result, the exact wall thickness has minimal impact on overall propagation behavior within this closed metallic structure. Features such as ridges, seams, lips, and structural flanges would likely produce a more significant influence on scattering and multipath propagation; however, accurately modeling these fine structural details would substantially increase computational complexity and simulation time beyond practical limits for this study.

4.2 Adding Antennas to the Railcar

Once the railcar was modeled, the antennas designed in CHAPTER III were added. The placement of the receiving antennas was determined by the locations of the wheel and axle assemblies on the train car. This was done to mimic the placement of wireless sensors used for bearing condition monitoring. For the boxcar, the distances used were 1.74 m (5.71 ft) between bogies and 8.77 m (28.77 ft) between wheelsets. As pictured in Figure 14, bogies sit beneath the railcar and hold two wheelsets together, with gravity supporting the weight of the railcar.

After adding the antennas simulating the sensors, the next hurdle was adding the antenna representing the gateway. A gateway is a communication hub that receives data from sensors, processes it, and relays the information to the cloud. In this case, the gateway must communicate with an antenna in the opposite bottom corner. The location chosen for these experiments was the top corner of the railcar, 6 cm above the roof. These spots were chosen to reduce the risk of someone tampering with the equipment after installation, and to help model worst-case scenario conditions for path loss.

4.3 Testing Antenna Performance with a Railcar Floating in Free Space

The initial simulation evaluated antenna performance on a single isolated railcar suspended in free space. This simplified scenario allowed the influence of the railcar structure to be studied without additional environmental effects.

An antenna was positioned λ/4 away from the railcar surface, where λ corresponds to the free-space wavelength at 915 MHz. For this design, λ/4 equals 7.09 cm (2.79 in). The λ/4 spacing was selected because it minimizes coupling between the antenna and the conductive railcar surface while maximizing radiation efficiency and allowing operation near its intended resonant characteristics.

Figure 15 gives the resulting computer-aided design (CAD) model. The corresponding S_{11} parameter response, represented in Figure 16, demonstrates that the presence of the railcar does not significantly detune the antenna. A strong S_{11} response is observed near the design frequency, confirming efficient power transfer between the transmitting and receiving antennas.

These results establish a baseline for evaluating more complex scenarios involving ground effects, ballast, and neighboring railcars.

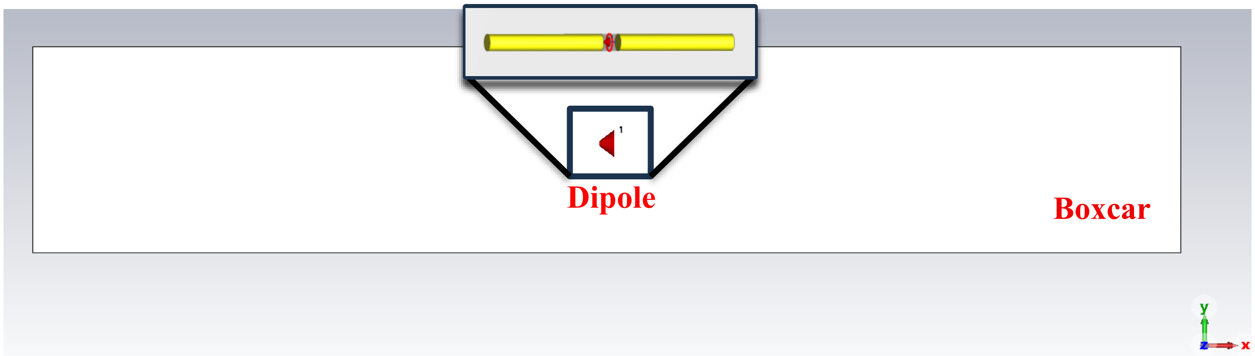

Figure 15: Railcar with antenna spaced λ/4 apart

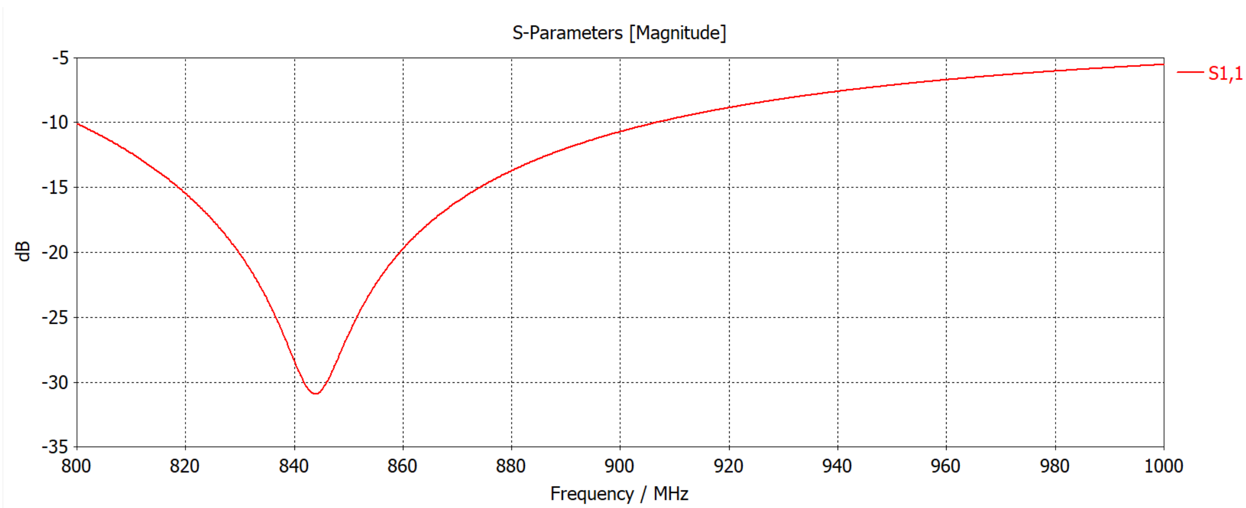

Figure 16: S-Parameters for Railcar with Antenna Spaced λ/4 apart Without Ground

4.4 Modeling Antennas on a Single Railcar in Free Space with Soil and Ballast

To more accurately represent real operating conditions, the free-space model was expanded to include both ballast and soil beneath the railcar. The ballast was modeled using a relative permittivity of 4.7, an electrical conductivity of 0.0001 S/m, and a relative permeability of 1. The soil was modeled with a relative permittivity of 3, an electrical conductivity of 0.001 S/m, and a relative permeability of 1. Figure 17 illustrates the complete simulation geometry, and its resulting S-parameter response is depicted in Figure 18.

Comparison with the free-space results reveals minimal change in antenna performance. Both the center frequency and the transmission coefficient remain nearly identical. This result indicates that the railcar itself dominates the electromagnetic behavior, while the influence of the ground, ballast, and soil is relatively small at the operating frequency. Consequently, subsequent simulations can focus primarily on railcar geometry and antenna placement without significant loss of accuracy.

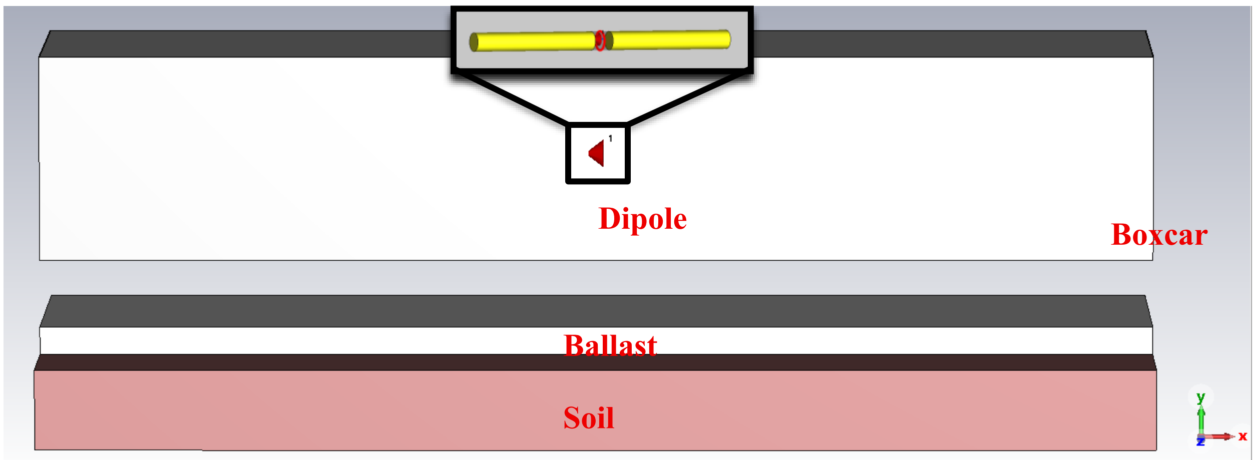

Figure 17: Railcar with Antenna Spaced λ/4 Apart with Soil and Ballast

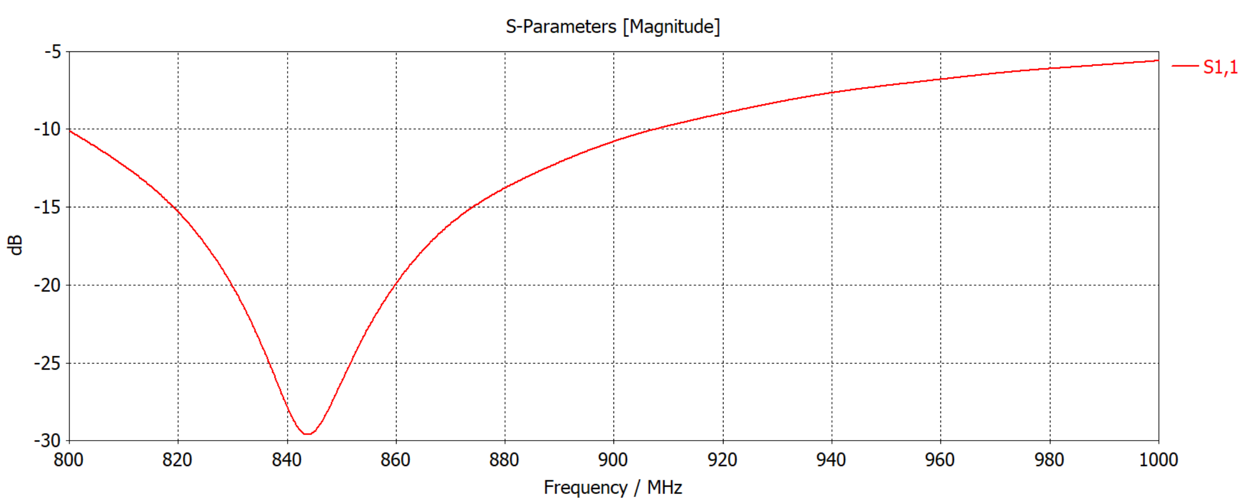

Figure 18: S-Parameters for Railcar with Antenna Spaced λ/4 Apart with Soil and Ballast

4.5 Testing Gateway Antenna at the Opposite Diagonal from the Sensor Antenna

After validating the antenna performance in the presence of a single railcar, the next step was to evaluate a realistic communication scenario representative of an onboard wireless sensor network. In this configuration, the sensing antenna was mounted beneath the railcar near one corner, corresponding to the physical location of a bearing-mounted sensor. The gateway antenna was positioned above the roof at the diagonally opposite corner of the railcar, representing one of the most challenging communication paths possible on a single car.

This arrangement was intentionally selected as a worst-case scenario. The transmitted signal must propagate around the metallic railcar structure while encountering significant reflection, diffraction, and scattering. These effects are particularly pronounced because the highly conductive steel surfaces dominate the railcar geometry.

Figure 19 illustrates the antenna placement used in this simulation. The resulting S-parameter response demonstrates that communication remains achievable despite the obstructed propagation path, as seen in Figure 20. Although the received power is substantially lower than that observed in line-of-sight configurations, the measured coupling remains within the sensitivity limits of modern LoRa transceivers.

These results confirm that reliable communication can be established even under highly unfavorable placement conditions. This finding is critical because actual sensor installations may not always permit ideal antenna orientation or direct visibility to the gateway.

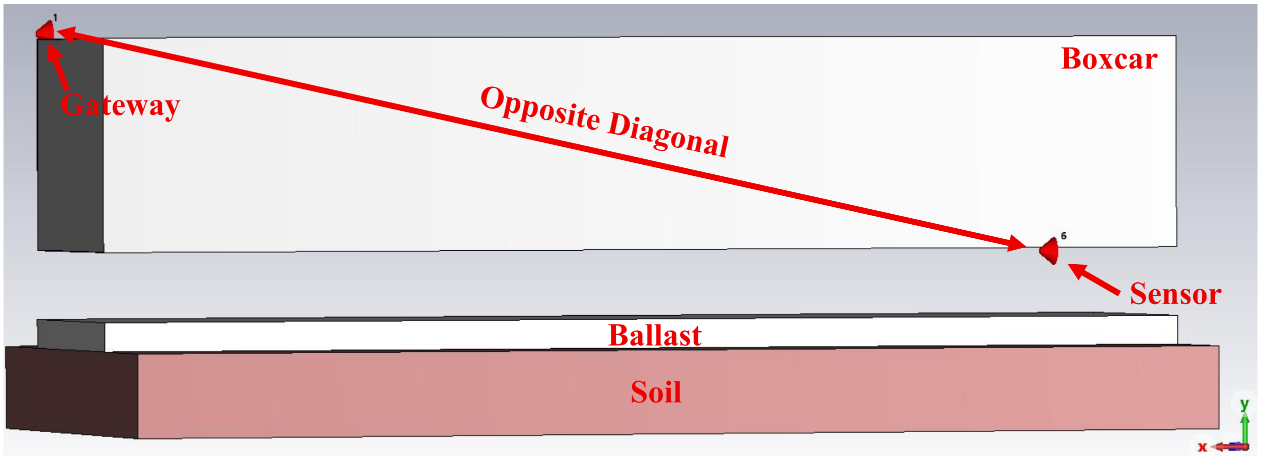

Figure 19: Gateway Antenna at the Opposite Diagonal from the Sensor Antenna

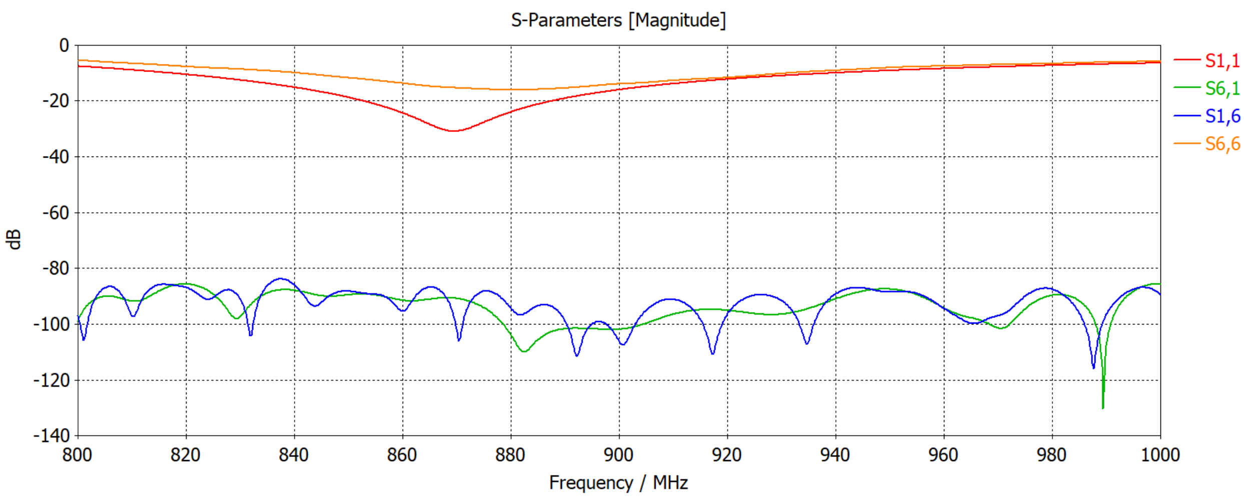

Figure 20: S-Parameters for Railcar with Antennas on Opposite Diagonals

4.6 Testing Various Antenna Polarizations

Antenna polarization significantly affects wireless communication performance, particularly in multipath-rich environments such as freight trains. To determine the optimal orientation, all possible combinations of orthogonal antenna polarizations were evaluated.

The first letter in each polarization pair denotes the sensor antenna orientation, while the second letter denotes the gateway antenna orientation. For example, "YX" indicates that the sensor antenna is vertically oriented along the y-axis, while the gateway antenna is oriented along the x-axis. Table 1 summarizes the median S_{21} values and their corresponding standard deviations for each polarization combination.

The results indicate that the YY configuration provides the strongest average coupling, with a median S_{21} value of -70.87 dB. The YX and YZ configurations also exhibit comparable performance. In contrast, the XX orientation produced the weakest coupling, with a median value of -96.04 dB.

These findings demonstrate that vertical polarization of the sensing antenna is highly advantageous in this application. The improvement is attributed to the geometry of the railcar and the orientation of the conductive surfaces, which favor vertically polarized fields. Additionally, the relatively low standard deviation observed in the YY configuration indicates consistent performance across the operating bandwidth and was selected as the preferred configuration for subsequent simulations.

Table 1: S-Parameter Table for Different Polarizations

S_{21} Polarization	S-Parameter Median dB	S-Parameter Standard Deviation dB
XX	-96.04	1.86
XY	-84.73	3.33
XZ	-82.83	3.20
YX	-72.71	1.84
YY	-70.87	3.67
YZ	-68.94	9.53
ZX	-77.02	2.70
ZY	-84.73	3.32
ZZ	-73.47	2.65

4.7 Placement of Sensing Antenna on Adapter Location

Although the initial sensor location was chosen to simplify modeling, practical implementation requires mounting the antenna on the bearing adapter. This location more accurately represents the intended deployment of the wireless sensing module.

To assess the impact of this relocation, the sensing antenna was repositioned to the adapter mounting location while maintaining the gateway antenna at the diagonally opposite rooftop position. The same polarization sweep described in Section 4.6 was then repeated.

The results, presented in Table 2, show a noticeable improvement across nearly all polarization combinations. The YY configuration again yielded the strongest performance, with an average S_{21} value of -68.41 dB, representing an improvement of approximately 3 dB over the previous location.

This enhancement can be attributed to the altered coupling between the antenna and the railcar structure. The adapter location provides a more favorable radiation environment, reducing destructive interference and improving the propagation path toward the gateway. The results confirm that the bearing adapter is an excellent mounting location, offering both practical installation advantages and improved wireless performance.

Table 2: S-Parameters Adjusted to Represent Adapter Location

S_{21} Polarization	S-Parameter Median dB	S-Parameter Standard Deviation dB
XX	-93.00	4.78
XY	-81.69	6.25
XZ	-79.79	6.12
YX	-69.67	4.76
YY	-67.83	6.60
YZ	-65.90	12.45
ZX	-73.98	5.62
ZY	-81.69	6.25
ZZ	-70.43	5.58

4.8 Testing Antenna Performance with Multiple Railcars

While single-car simulations provide valuable insight, freight trains consist of many interconnected railcars. The presence of adjacent cars can significantly alter the electromagnetic environment through additional reflections and waveguiding effects.

To investigate these phenomena, multiple-railcar simulations were conducted. In all cases, the sensing antenna was mounted beneath the railcar at the adapter location, and the gateway antenna was placed above the railcar at the opposite diagonal corner. This configuration represents the worst-case single-car communication path identified earlier. Two scenarios were considered for these simulations: an additional railcar placed adjacent to the gateway side and an additional sensor placed adjacent to the sensor side. These simulations were designed to determine whether neighboring railcars either enhance or degrade communication performance.

4.8.1 Testing Antenna Performance by Placing an Extra Railcar Next to the Gateway Antenna

In the first scenario, a second railcar was positioned immediately next to the gateway side of the primary railcar, as shown in Figure 21. The additional metallic structure acts as a large reflective surface, redirecting energy toward the receiving antenna. This creates a partial waveguide effect that improves signal confinement and reduces radiative losses. The median S_{21} improved to -89.10 dB, representing a substantial enhancement compared to the isolated railcar case.

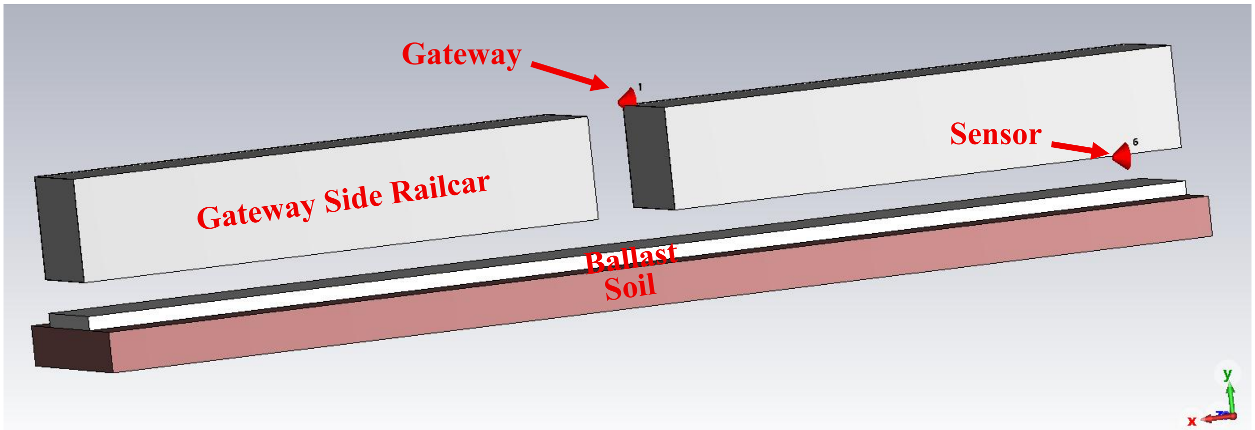

Figure 21: Extra Railcar on Gateway Antenna Side

4.8.2 Testing Antenna Performance by Placing an Extra Railcar Next to the Sensor Antenna

In the second scenario, the additional railcar was positioned adjacent to the sensor side, as illustrated in Figure 22. Although improvement was still observed, the effect was less pronounced than in the gateway-side configuration. The median S_{21} (transmission coefficient) increased to -97.81 dB. This difference occurs because reflections near the receiving antenna contribute more directly to improved coupling than reflections near the transmitting antenna.

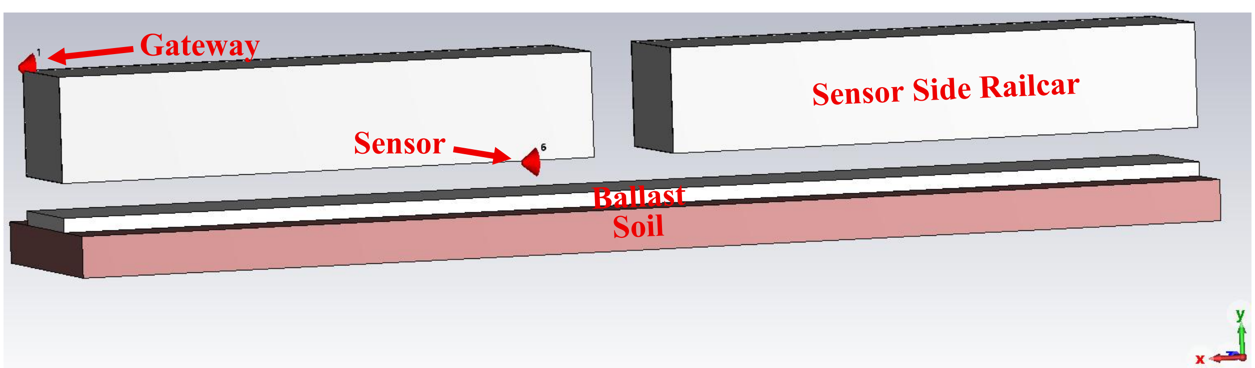

Figure 22: Extra Railcar on Sensor Antenna Side

4.8.3 Comparison of Multiple Railcar Configurations

Table 3 summarizes the results of the multiple-railcar simulations. The isolated railcar produced a median S_{21} of -96.04 dB. Adding a neighboring railcar improved performance in both cases, with the gateway-side placement yielding the largest benefit. These findings suggest that the presence of adjacent railcars can enhance wireless communication by creating additional reflective paths and waveguiding effects. Since freight trains naturally operate as multi-car consists, field service performance is expected to exceed that predicted by isolated single-car simulations. This result is particularly encouraging for practical deployment, as it indicates that communication reliability may improve as train length increases.

Table 3: S-Parameter Comparison from Extra Railcars

Extra Car Side	S-Parameter Median dB	S-Parameter Standard Deviation dB
Gateway	-89.10	6.14
Sensor	-97.81	5.00
No Car	-96.04	5.51

CHAPTER V

FIELD TESTING

5.1 Setting up Field Tests

To validate the simulation results presented in CHAPTER IV, field testing was conducted on an operational hopper railcar. Permission to perform these tests was obtained from a local short-line railroad. Two antennas, designed and fabricated according to the specifications presented in CHAPTER III, were used during the field experiments.

The primary difference between the simulated and experimental configurations was the inclusion of a 4.57 m (15 ft) RG58 coaxial cable with SMA male connectors. At 915 MHz, this cable introduces approximately 2 dB of insertion loss, which was measured experimentally and later accounted for during data post-processing.

A Rohde & Schwarz ZNL6 Vector Network Analyzer / Spectrum Analyzer was first used to characterize the fabricated antennas and verify impedance matching and resonance near the intended operating frequency. The measured S_{11} (reflection coefficient) parameter of the fabricated antenna is shown in Figure 23. The results indicate that the antenna resonates near 915 MHz with acceptable return loss, confirming proper impedance matching and validating consistency with the simulated design presented in CHAPTER III.

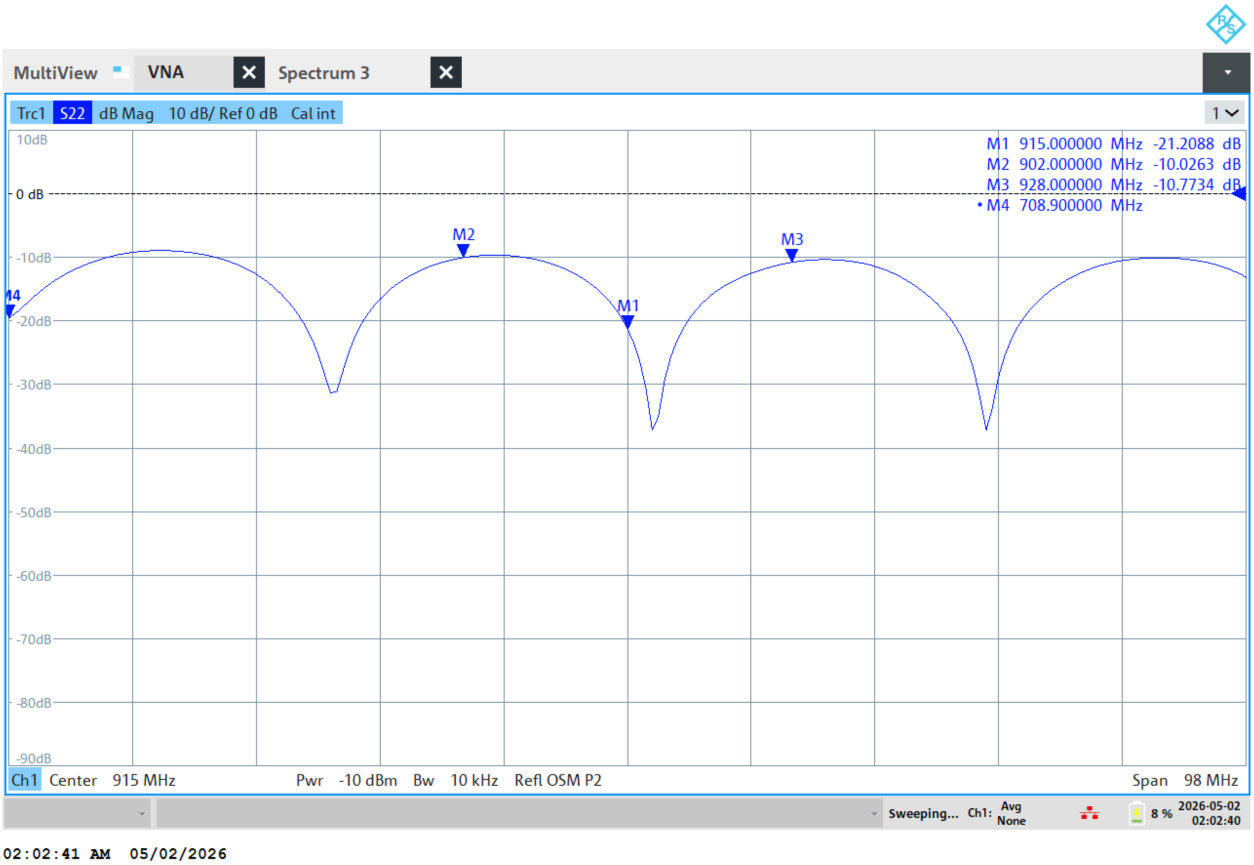

Figure 23: 915MHz Antenna S_{11} (reflection coefficient) Parameter

Although minor deviations between simulated and measured S_{11} responses were observed, these differences were expected due to fabrication tolerances, connector effects, and environmental influences during measurement. Afterwords, another identical antenna was created to properly test communication. Overall, the measured S_{11} response confirms that the antenna is suitable for field deployment and that any discrepancies observed in later measurements were not due to antenna mismatch.

Once antenna performance was validated, one antenna was connected to a Rohde & Schwarz SMCV100B Vector Signal Generator, while the second antenna was connected to the spectrum analyzer. Prior to deployment in the railyard, the complete wireless link was tested at the University of Texas Rio Grande Valley to verify proper system operation.

The simulation studies presented in CHAPTER IV were performed using a boxcar model, whereas the experimental measurements in this chapter were conducted on a hopper railcar. This difference was due to the availability of railcars at the short-line railroad facility where field testing was performed. Although the geometries of the two railcar types differ, both consist primarily of large metallic structures that create similar reflective and obstructive propagation environments. Consequently, meaningful comparison between simulation and experimental results remains possible despite the differences in railcar design.

Field testing was then conducted using the hopper railcar, as seen in Figure 24. The physical placement of the test equipment is illustrated in Figure 24 through Figure 27. The transmitting antenna was mounted near the L1 bearing adapter location, as shown in Figure 28 and Figure 29, while the gateway antenna was mounted on the upper portion of the railcar, as delineated in Figure 26 and Figure 27. Figure 30 helps illustrate the bearing locations along the railcar for mounting the sensors.

Figure 24: Field Tested Hopper Car

Figure 25: Vector Signal Generator Field Test Location

Figure 26: Hopper Car Side Profile with Test Equipment

Figure 27: Gateway Antenna X Axis Mount Location

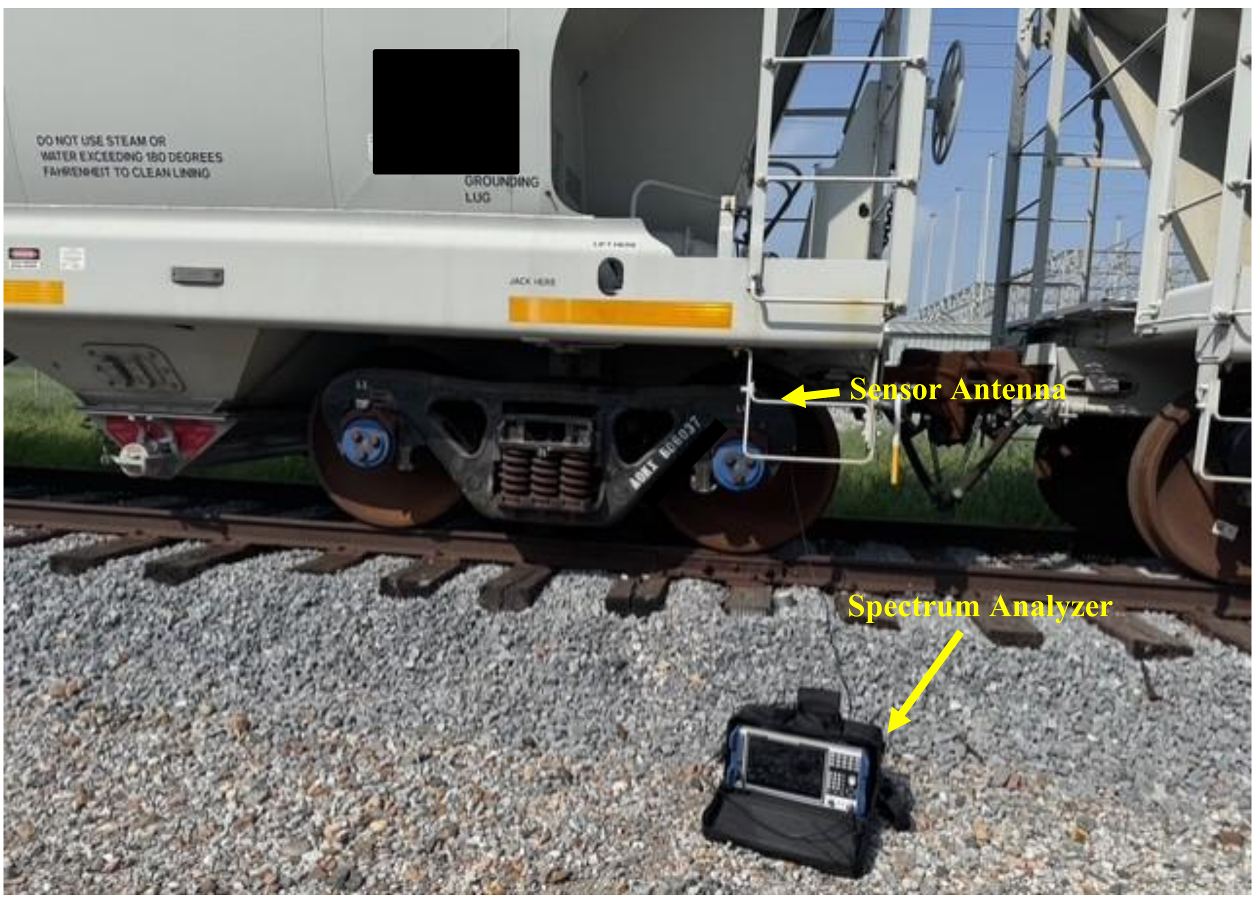

Figure 28: Field Test Setup with Antenna on L1 Location Above the Bogie

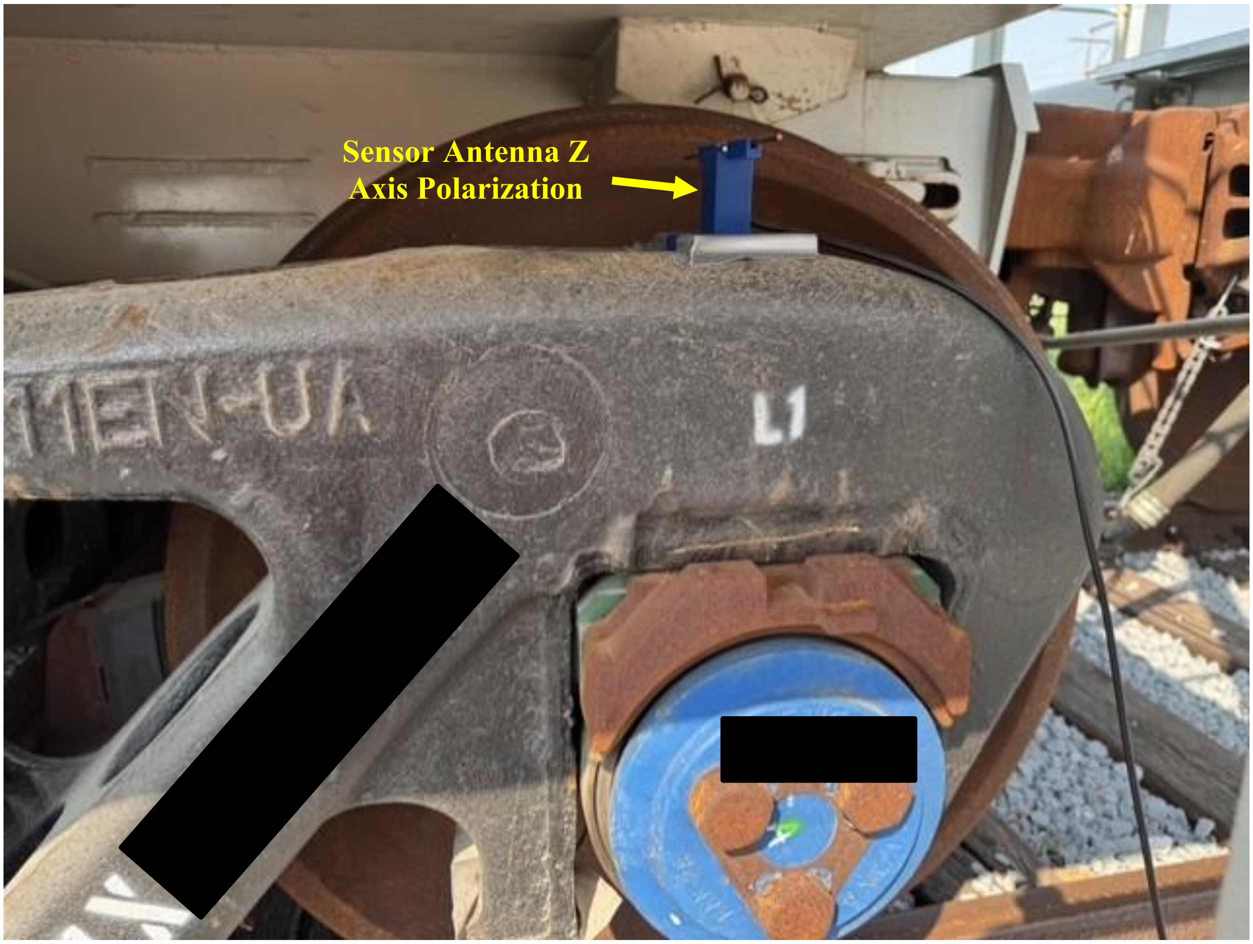

Figure 29: Sensor Antenna Located on top of L1 Bearing Position Above the Bogie

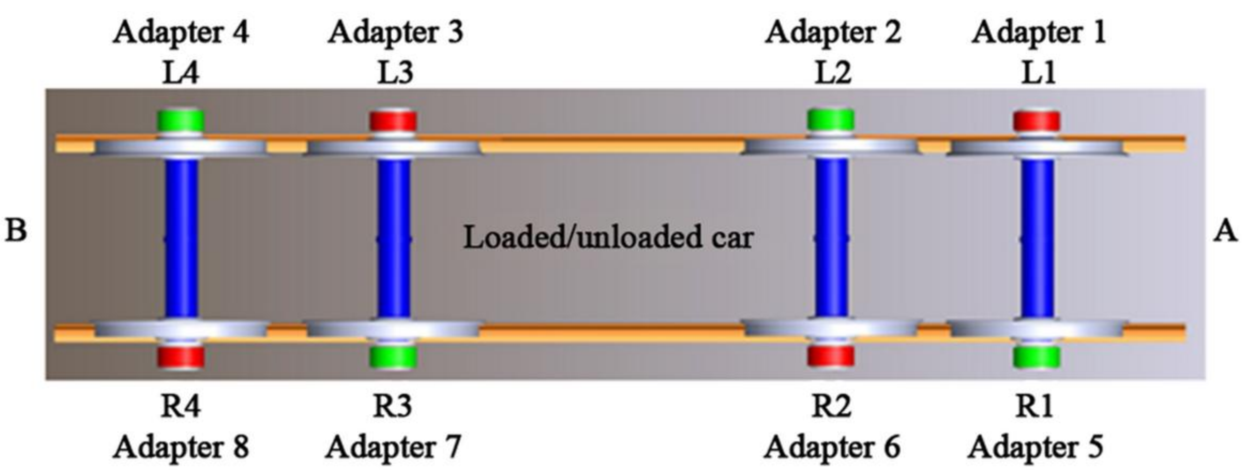

Figure 30: Railcar Adapter Naming and Locations [12]

The hopper railcar used during testing had approximate dimensions of 16.76 m (55 ft) in length, 3.05 m (10 ft) in width, and 4.57 m (15 ft) in height. These dimensions differ from those used in the simulations and may introduce variations in propagation behavior due to changes in geometry, reflection paths, and scattering characteristics. This configuration closely replicates the worst-case communication scenario analyzed in CHAPTER IV, enabling direct comparison between simulated and measured antenna performance.

5.2 Testing Antenna Polarizations

After establishing the field test setup, measurements were conducted for multiple antenna polarization configurations to characterize the wireless channel between the sensing antenna and the gateway antenna.

During each test, the vector signal generator swept across the 902 MHz to 928 MHz frequency range using a linear step size of 1 MHz. This sweep fully covers the 915 MHz ISM band while providing sufficient resolution for statistical analysis. The spectrum analyzer recorded the received signal strength at each frequency point.

Figure 31 shows a representative spectrum analyzer plot, where a distinct peak is observed at 915 MHz, confirming successful signal transmission and reception. However, instead of relying on a single frequency point, a broader set of measurements was carried out.

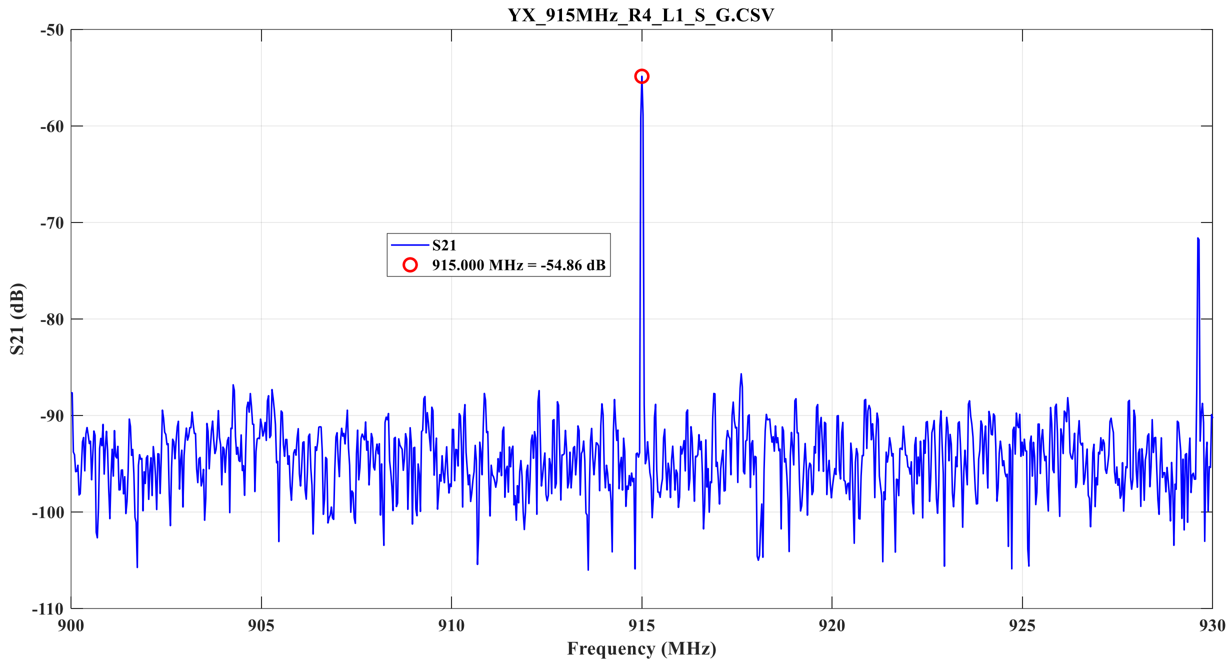

Figure 31: 915MHz Spectrum Analyzer Plot

To account for variations in the wireless channel, the received power values across the frequency sweep were extracted and aggregated. Figure 32 shows the resulting S_{21} sweep, along with the calculated median and standard deviation. This approach provides a more robust characterization of antenna performance compared to single-frequency measurements.

Cable losses were also measured separately using the vector network analyzer, as presented in Figure 33. At 915 MHz, the total cable loss was approximately 2 dB. This loss was added back to the measured received power to obtain corrected S_{21} values.

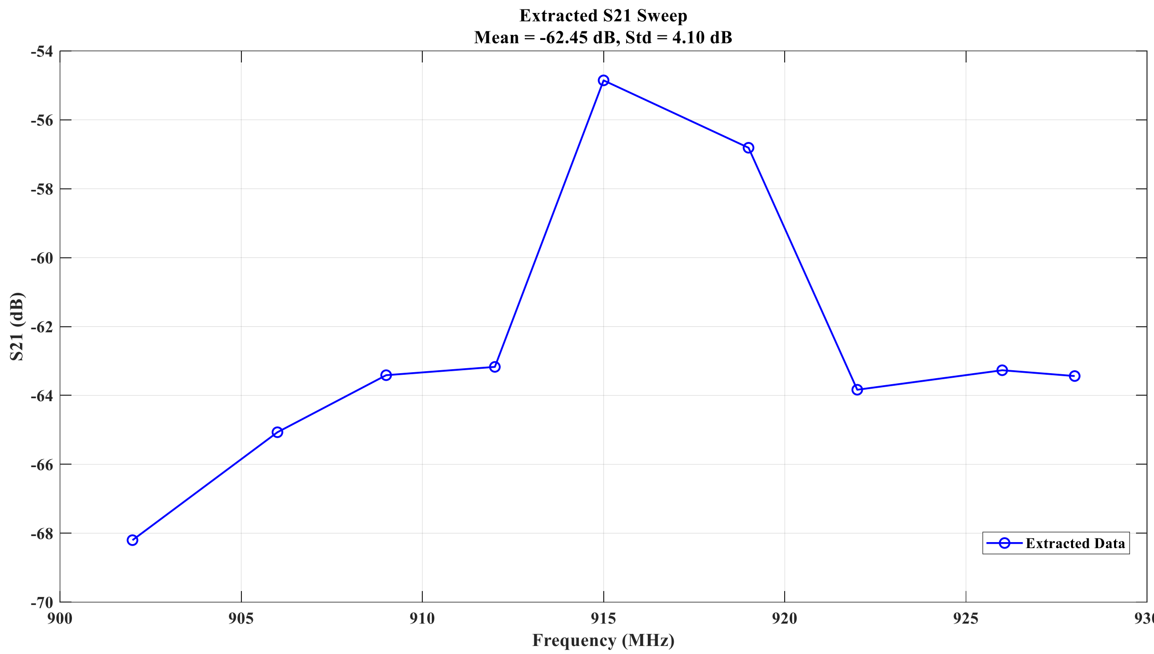

Figure 32: Aggregate S_{21} (Transmission Coefficient) Parameter from Spectrum Analyzer Data

Figure 33: Antenna Cable Loss

Due to battery limitations of the portable measurement equipment, only six of the nine possible polarization combinations were tested. Specifically, configurations requiring Y-axis polarization at the gateway antenna (YX, YY, and YZ) were not measured.

5.3 Comparing Simulation vs Field Tests

Table 4 summarizes the measured S_{21} values obtained during field testing after accounting for cable losses. These values represent the median received power and variability across the 902–928 MHz frequency sweep for each tested polarization configuration.

Table 4: Field Results S-Parameter Polarization Table Accounting for Losses

S_{21} Polarization	S-Parameter Median dB	S-Parameter Standard Deviation dB
XX	-72.39	4.44
XY	N/A	N/A
XZ	-71.6	4.57
YX	-65.41	4.1
YY	N/A	N/A
YZ	-70.47	5
ZX	-65.01	3.49
ZY	-72.39	4.44
ZZ	N/A	N/A

To better approximate field operating conditions, the simulation model was extended to include a neighboring railcar positioned adjacent to the sensing antenna. The resulting simulated S-parameter values are summarized in Table 5 alongside the field data for comparison.

Table 5: Field and Simulation Result Comparison

S_{21} Polarization	S-Parameter Median Field dB	S-Parameter Median Simulation dB	Standard Deviation Field dB	Standard Deviation Simulation dB
XX	-72.39	-96.04	4.44	1.34
XY	N/A	-84.73	N/A	2.81
XZ	-71.6	-82.83	4.57	2.68
YX	-65.41	-72.71	4.1	1.32
YY	N/A	-70.87	N/A	3.16

(Table 5 continued)

YZ	-70.47	-68.94	5	9.01
ZX	-65.01	-77.02	3.49	2.18
ZY	N/A	-84.73	5	2.81
ZZ	-72.21	-73.47	3.2	2.14

A comparison of the results reveals a notable discrepancy between simulation and field measurements. A comparison between the simulated and measured results shows that several polarization configurations experienced substantial improvement during field testing. In particular, the XX, XZ, YX, and ZX configurations exhibited significantly stronger received signal levels in the field than predicted by simulation. The largest improvement was observed in the XX configuration, where the median S_{21} improvedfrom -96.04 dB in simulation to -72.39 dB during field testing, representing an increase of approximately 23.65 dB. Similarly, the XZ and ZX configurations improved by approximately 11.23 dB and 12.01 dB, respectively. The YX configuration also demonstrated an improvement of approximately 7.30 dB.

This difference can be attributed primarily to multipath propagation effects present in the railyard environment. Figure 25 through Figure 30 depict the presence of additional railcars, track infrastructure, and surrounding metallic structures that introduce numerous reflection paths. These reflections can constructively interfere with the received signal, significantly increasing the measured signal strength. One strong piece of evidence for significant multipath components is the consistently higher standard deviation in the measurements compared to simulations. Multipath causes pseudo-random variation in S_{21} with frequency, with the frequency scale of the variations roughly determined by when the round-trip difference is one-half wavelength. Multiple other railcars 20 m away would be expected to cause noticeable variations when the frequency changes by 3.75 MHz, which is consistent with the data presented in Figure 28.

In particular, horizontally oriented electric field components (X and Z polarizations) were more likely to interact with other cars due to the long, straight horizontal edges of the car, leading to enhanced coupling that is not fully captured in the simulation model. This explains the improved performance of XX, XY, and XZ configurations in field measurements.

Additional discrepancies arise from antenna alignment and mounting conditions. While simulations assume ideal positioning, practical implementations introduce slight misalignments and surface irregularities that result in polarization mixing. This effect allows energy from one polarization to be partially received by another, further increasing measured signal strength.

Material properties also differ between simulation and reality. The CST Studio Suite model assumes uniform material characteristics, whereas the actual railcar includes variations such as paint, corrosion, welds, and structural discontinuities. These features contribute to additional scattering and redistribution of electromagnetic energy.

Furthermore, the hopper railcar used in field testing differs geometrically from the boxcar used in simulation. These differences alter reflection paths and may contribute to variations in measured performance.

Although the Y-axis gateway polarization configurations (YX, YY, and YZ) were not measured due to equipment limitations, their expected performance can be inferred from simulation results. The simulation indicates that these configurations, particularly YY and YX, provide strong coupling due to alignment with the vertical structure of the railcar.

In the field environment, it is likely that these configurations would also exhibit strong performance. However, the influence of multipath propagation may reduce their relative advantage. The enhanced coupling observed in X and Z polarizations suggests that field conditions tend to distribute energy more evenly across polarization states than predicted by the simulations.

Overall, while the simulations do not perfectly predict the absolute values observed in field testing, they successfully capture the general behavior of the system and provide valuable insight into antenna placement and environmental effects. The discrepancies observed highlight the importance of experimental validation when designing wireless systems for complex and highly reflective environments.

5.4 Summary of Results

The field testing results confirm that reliable wireless communication can be achieved between the sensing antenna and gateway antenna under realistic railroad operating conditions. Although differences exist between simulation and measured results, these discrepancies are well explained by environmental complexity, multipath propagation, and practical implementation factors. Notably, field performance in several cases exceeded simulation predictions due to constructive interference and additional propagation paths. The results also demonstrate that antenna polarization behavior in railyard environments is influenced by surrounding structures and cannot be fully predicted using simplified models alone. Overall, the proposed antenna system demonstrates strong potential for deployment in railroad applications, providing robust wireless connectivity and sufficient link margin across multiple operating conditions.

CHAPTER VI

CONCLUSIONS AND FUTURE WORK

6.1 Conclusions

This thesis investigated wireless signal propagation between a sensing antenna mounted near the bearing location and a gateway antenna on a freight railcar. The primary objective was to determine how antenna polarization and placement influence received signal strength in a realistic rail environment and to quantify these effects using both simulation and field testing.

Through electromagnetic simulation, various antenna polarization configurations were evaluated under controlled conditions. These simulations provided an initial understanding of how railcar geometry, antenna orientation, and the presence of neighboring railcars influence signal propagation. In particular, the results demonstrated that polarization alignment relative to the railcar structure plays a significant role in determining path loss.

Field testing was conducted on an operational hopper railcar to validate these findings. A frequency sweep across the 902–928 MHz ISM band was used to capture received signal strength over multiple frequency points, allowing the calculation of both median and standard deviation for each polarization configuration. This approach provided a statistically meaningful representation of channel behavior rather than relying on a single-frequency measurement.

The experimental results confirmed that reliable wireless communication is achievable within the railcar environment. However, the field measurements also revealed important differences from simulation. Polarization configurations that exhibited weaker performance in simulation, particularly XX, XY, and XZ, showed significantly stronger performance in the field.

This behavior is attributed to multipath propagation and reflections from surrounding railcars and infrastructure, which enhance signal strength in ways not fully captured by the simulation model.

The most significant outcome of this work is the quantified relationship between polarization configuration and received signal strength, expressed through median S_{21} values and their associated standard deviations. These results provide practical insight into both the expected signal level and its variability across the operating frequency band. The inclusion of standard deviation is particularly important, as it reflects channel variation and informs the design of reliable communication systems.

From a system perspective, these findings have direct implications for power optimization. By identifying polarization configurations that consistently produce higher median received power, it becomes possible to reduce transmit power while maintaining reliable communication. This reduction in required transmit power directly translates to lower energy consumption, which is critical for battery-powered onboard sensing devices.

Additionally, the observed variability across the frequency sweep provides guidance for frequency hopping strategies in systems such as LoRa. Polarization configurations with lower standard deviation indicate more stable channels, which may allow for reduced hopping or more predictable performance. Conversely, higher variability suggests the need for more aggressive frequency diversity to maintain reliable communication.

Overall, this work establishes a set of experimentally validated polarization-dependent propagation characteristics for railcar environments. These results provide a practical foundation for optimizing wireless onboard communication systems in terms of both power efficiency and reliability.

To further enhance the practical applicability of these results, future improvements should focus on increasing system efficiency and developing predictive design tools. In particular, the use of directional antennas offers the potential to concentrate radiated energy along dominant communication paths, reducing power consumption while improving link performance. Additionally, the statistical characterization of the channel presented in this work provides a foundation for developing empirical loss models that can be used to estimate signal strength and optimize system parameters without requiring full-wave simulation.

6.2 Contributions

The primary contribution of this research is the experimental characterization of polarization-dependent wireless propagation on freight railcars, supported by both simulation and field validation. Unlike prior work that focuses primarily on antenna design or generalized propagation models, this study provides quantitative data that can be directly applied to system-level design.

A key contribution is the determination of median S_{21} (transmission coefficient) values for multiple polarization configurations within a realistic rail environment. These values provide a direct measure of expected signal strength for different antenna orientations, enabling informed decisions about antenna placement and alignment in practical deployments.

Equally important is the inclusion of standard deviation as a performance metric. By quantifying variability across the operating frequency band, this work captures the effects of multipath propagation and frequency-selective fading. This information is critical for designing robust communication systems, as it provides insight into channel stability rather than relying solely on average performance.

Another significant contribution is the comparison between simulation and field measurements, which highlights the limitations of simplified electromagnetic models in highly reflective environments. The observed discrepancies demonstrate that practical propagation conditions can enhance signal strength through multipath effects, particularly for certain polarization configurations. This finding emphasizes the importance of incorporating experimental validation into the design process.

Finally, this research provides practical guidance for optimizing wireless communication systems on railcars. The results can be directly used to reduce transmit power requirements, improve energy efficiency, and inform frequency hopping strategies in low-power communication protocols such as LoRa. In this way, the work moves beyond theoretical analysis and delivers actionable insights for the development of onboard sensing technologies.

6.3 Limitations

While the results of this study provide valuable insight into wireless propagation on railcars, several limitations should be acknowledged.

The simulation environment, although detailed, does not fully capture the complexity of an operational railyard. While neighboring railcars were included in later simulations, additional environmental factors such as multiple adjacent cars, track structures, and surrounding infrastructure were not comprehensively modeled. These elements contribute to multipath propagation and may influence the observed discrepancies between simulation and field results.

The railcar used in field testing also differed in geometry from the model used in simulation. Variations in dimensions and structural features can alter reflection paths and scattering behavior, which may affect signal propagation.

Additionally, not all polarization configurations were tested in the field due to equipment limitations. Specifically, configurations involving Y-axis polarization at the gateway antenna were not measured. Although their behavior can be inferred from simulation, direct experimental validation would strengthen the conclusions.

Finally, the analysis focused on received signal strength as the primary performance metric. While this provides a strong indication of link feasibility, additional system-level metrics such as packet delivery rate, latency, and error performance were not evaluated.

6.4 Future Work

Future work should focus on extending this research toward improved system efficiency and predictive modeling of wireless communication performance in railcar environments.

One important direction is the evaluation of directional antennas in place of the omnidirectional dipole antennas used in this study. While omnidirectional antennas provide broad coverage, they also distribute radiated power in directions that do not contribute to communication between the sensing antenna and the gateway. Directional antennas offer the potential to concentrate energy along the primary communication path, thereby increasing received signal strength and reducing unnecessary power loss.

Testing directional antennas in the same railcar configuration would provide insight into how beam shaping influences propagation in a highly reflective environment. In particular, it would be valuable to determine whether directional gain can improve link reliability while reducing transmit power requirements. However, such antennas may also be more sensitive to misalignment and multipath effects, making it necessary to evaluate their performance under realistic mounting conditions and varying orientations.

Another key area for future work is the development of an empirical loss model for wireless propagation on railcars. The results presented in this thesis provide measured median S_{21} values and associated standard deviations for multiple polarization configurations. This data can serve as the foundation for constructing a predictive model that relates received signal strength to antenna orientation, placement, and environmental conditions.

A loss model could incorporate both deterministic components, such as geometric path loss and antenna alignment, and statistical components derived from the measured variability across the frequency band. Such a model would enable system designers to estimate expected signal strength and required transmit power without relying solely on full-wave electromagnetic simulation.

The combination of directional antenna optimization and a validated loss model would significantly enhance the practical applicability of this research. Together, these approaches would allow for more efficient system design by reducing power consumption, improving link reliability, and enabling more accurate prediction of wireless performance in physical environments.

6.5 Final Remarks

This thesis demonstrates that wireless communication in the challenging environment of a freight railcar can be effectively characterized through a combination of simulation and field testing. More importantly, it provides quantitative results that can be directly applied to the design of onboard wireless sensing systems.

By focusing on polarization-dependent performance and statistical characterization of the channel, this work offers practical guidance for optimizing power usage and communication reliability. These contributions support the development of more efficient, robust, and scalable wireless systems for railway applications.

REFERENCES

[1] L. Cantu, "Assessing the Effectiveness and Efficacy of Wireless Onboard Condition Monitoring Modules in Identifying Defects in Railroad Rolling Stock," *Theses Diss.*, Dec. 2021, [Online]. Available: https://scholarworks.utrgv.edu/etd/839

[2] "2.09 - Train Accidents Trend." Accessed: Feb. 01, 2026. [Online]. Available: https://safetydata.fra.dot.gov/officeofsafety/publicsite/query/TrainAccidentsFYCYWithRates.aspx

[3] "Norfolk Southern Railway Derailment and Hazardous Materials Release, East Palestine, Ohio, February 3, 2023".

[4] "NATIONWIDE WAYSIDE DETECTOR SYSTEM - PDF Free Download." Accessed: Mar. 12, 2026. [Online]. Available: https://docplayer.net/17829351-Nationwide-wayside-detector-system.html

[5] S. Karunakaran and T. W. Snyder., "Bearing temperature performance in freight cars," presented at the Bearing Research Symposium, AAR Research Program in conjunction with the ASME RTD Fall Conference, Chicago, IL, September 11-12.

[6] C. Tarawneh, J. Aranda, V. Hernandez, S. Crown, and J. Montalvo, "An investigation into wayside hot-box detector efficacy and optimization," *Int. J. Rail Transp.*, vol. 8, no. 3, pp. 264–284, Jul. 2020, doi: 10.1080/23248378.2019.1636721.

[7] G. B. Anderson, "Acoustic Detection of Distressed Freight Car Roller Bearings," presented at the ASME/IEEE 2007 Joint Rail Conference and Internal Combustion Engine Division Spring Technical Conference, American Society of Mechanical Engineers Digital Collection, Jun. 2009, pp. 167–171. doi: 10.1115/JRC/ICE2007-40091.

[8] "An Implementation Guide for Wayside Detector Systems | FRA." Accessed: Mar. 12, 2026. [Online]. Available: https://railroads.dot.gov/elibrary/implementation-guide-wayside-detector-systems

[9] "The trackside acoustic detection system.," ResearchGate. Accessed: Apr. 24, 2026. [Online]. Available: https://www.researchgate.net/figure/The-trackside-acoustic-detection-system_fig1_374719860

[10] "RailBAM | Wabtec Corporation." Accessed: Mar. 12, 2026. [Online]. Available: https://www.wabteccorp.com/digital-intelligence/condition-monitoring/kinetix-inspection-technologies/wayside/railbam

[11] “Overview of the new RailBAM Acoustic Bearing Monitor,” Rail Geelong. Accessed: Apr. 24, 2026. [Online]. Available: https://www.railgeelong.com/gallery/geelong-line/lara-wild/E113_2270.jpg.html

[12] C. Tarawneh, J. Montalvo, and B. Wilson, “Defect detection in freight railcar tapered-roller bearings using vibration techniques,” *Railw. Eng. Sci.*, vol. 29, no. 1, pp. 42–58, Mar. 2021, doi: 10.1007/s40534-020-00230-x.

[13] J. Pams, C. Tarawneh, J. Montoya, B. Wilson, L. Cantu, and H. Alkhaldi, “Railroad Track and Wheel Defect Detection With Onboard Condition Monitoring System,” *Proc. 2024 Jt. Rail Conf. 2024 Jt. Rail Conf.*, Jun. 2024, doi: 10.1115/JRC2024-129911.

[14] M. Centenaro, L. Vangelista, A. Zanella, and M. Zorzi, “Long-range communications in unlicensed bands: the rising stars in the IoT and smart city scenarios,” *IEEE Wirel. Commun.*, vol. 23, no. 5, pp. 60–67, Oct. 2016, doi: 10.1109/MWC.2016.7721743.

[15] U. Raza, P. Kulkarni, and M. Sooriyabandara, “Low Power Wide Area Networks: An Overview,” Jan. 11, 2017, *arXiv*: arXiv:1606.07360. doi: 10.48550/arXiv.1606.07360.

[16] T. S. Rappaport, *Wireless communications: principles and practice*, 2nd ed. in Prentice Hall communications engineering and emerging technologies series. Upper Saddle River, N.J: Prentice Hall PTR, 2002.

[17] C. Balanis, *Antenna Theory: Analysis and Design, 4th ed.*, 4th ed. Wiley, 2016.

[18] C. A. Sanches, A. F. H. Librantz, and P. A. Belan, “Radio Propagation in Railway Corridors Through Dense Forests–Measurement and Modeling at 460 MHz”, doi: 10.1029/2025RS008362.

[19] H. Sharif and M. Hempel, “Study of RF Propagation Characteristics for Wireless Sensor Networks in Railroad Environments,” *-Am. Transp. Cent. Final Rep. Tech. Briefs*, Jan. 2010, [Online]. Available: https://digitalcommons.unl.edu/matcreports/40

[20] L. Zhang *et al.*, “Propagation modeling for outdoor-to-indoor and indoor-to-indoor wireless links in high-speed train,” *Measurement*, vol. 110, pp. 43–52, Nov. 2017, doi: 10.1016/j.measurement.2017.06.014.

[21] “Boxcars,” TrinityRail. Accessed: May 10, 2026. [Online]. Available: https://www.trinityrail.com/railcars/boxcars/

VITA

Dario Hinojosa was born in McAllen, Texas, on August 30, 2002. He attended James "Nikki" Rowe High School, where he participated in the International Baccalaureate Program at Lamar Academy and graduated in the top 14% of his class in 2020. He received his Bachelor of Science in Electrical Engineering from the University of Texas Rio Grande Valley (UTRGV) in 2024, during which time he had the distinct honor of being selected as a Commencement Bell Ringer. A Meritorious Scholar, Dario also received various other academic scholarships.

Throughout his tenure at UTRGV, Dario demonstrated extensive leadership and service. He served as the Vice President of the IEEE Edinburg Student Branch for the 2023-2024 academic year and as Program Director from 2022-2023. He was also a member of the Engineering Student Advisory Council from 2024–2026. In addition to his leadership roles, Dario served as a laboratory assistant for the Electrical Engineering Lab I and was a member of the University Transportation Center for Railway Safety for three years. Dario completed his Master of Science in Electrical Engineering in May 2026, where he was once again honored as a Commencement Bell Ringer. He can be reached via email at dariohinojosa73@gmail.com.